Journal of Inorganic Biochemistry 244 (2023) 112232

Contents lists available at ScienceDirect

Journal of Inorganic Biochemistry

journal homepage: www.elsevier.com/locate/jinorgbio

Vanadium(IV) complexes of salicylaldehyde-based furoic acid hydrazones: Synthesis, BSA binding and *in vivo* antidiabetic potential

Adnan Zahirović [a,*], Selma Hadžalić [a], Aleksandar Višnjevac [b], Muhamed Fočak [c], Burak Tüzün [d], Dijana Žilić [b], Sunčica Roca [b], Jurica Jurec [b], Anela Topčagić [a], Irnesa Osmanković [a]

[a] Laboratory for Inorganic and Bioinorganic Chemistry, Department of Chemistry, Faculty of Science, University of Sarajevo, Sarajevo, Bosnia and Herzegovina
[b] Ruđer Bošković Institute, Zagreb, Croatia
[c] Department of Biology, Faculty of Science, University of Sarajevo, Sarajevo, Bosnia and Herzegovina
[d] Plant and Animal Production Department, Technical Sciences Vocational School of Sivas, Sivas Cumhuriyet University, Sivas, Turkey

ARTICLE INFO

Keywords:
Vanadium(IV) hydrazone complexes
Salicylaldehyde
2-furoic acid
BSA binding affinity
Antidiabetic *in vivo* potential
Swiss-ADME analysis

ABSTRACT

Solution synthesis afforded five novel neutral heteroleptic octahedral paramagnetic mononuclear oxidovanadium(IV) complexes of general composition [VO(*bpy*)L], where L is a dianionic tridentate ONO-donor hydrazone ligand derived from 2-furoic acid hydrazide and salicylaldehyde and its 5-substituted derivatives. Characterization was carried out by elemental analysis, mass spectrometry, infrared, electron, NMR, and EPR spectroscopy, cyclic voltammetry and conductometry. The molecular and crystal structure of the complex with 5-chlorosalicylaldehyde 2-furoic acid hydrazone (**2**) was determined. The quantum chemical properties of the vanadium complexes were studied at B3LYP and M062X levels with the lanl2dz basis set using Gaussian. Additionally, Swiss-ADME analysis was performed and complex (**4**), featuring a 5-nitro substituent on the hydrazone ligand, was selected for further investigation. The effects of the *in vivo* application of the complex on selected biochemical parameters in healthy and diabetic Wistar rats were investigated. Strong antidiabetic effect associated with moderate hypoalbuminemia was observed. Furthermore, the interaction of complexes with BSA was studied by spectrofluorimetry. A significant conformational change of BSA in the presence of vanadium complexes was found. Synchronous fluorescence spectra revealed significant changes in the tyrosine microenvironment of BSA. The FRET analysis was also used and the non-radiative process of energy transfer is elucidated. Thermodynamic data suggest van der Waals forces and hydrogen bonding as predominant binding modes of complexes to BSA.

1. Introduction

The increasing interest in medicinal chemistry and drug discovery vividly illustrates how far is modern society from fast, reliable, and efficient drug discovery, which must rely on precisely established synthesis–structure–activity relationships. This poses inorganic chemists the challenging task of designing suitable metal-based drugs with predictable and desirable biological activities, which can be reasonably correlated to interactions with predefined biomolecular targets. In this context coordination complexes of vanadium are of great interest in the

Abbreviations: acac, Acetylacetonate; ADME, Absorption, Distribution, Metabolism, and Excretion; ALB, Albumins; bpy, 2,2′-bipyridine; BSA, Bovine serum albumin; BUN, Urea; COSY, Correlation spectroscopy; CYP, Cytochromes P450; CYP2C19, Cytochrome P450 2C19; DMF, *Dimethylformamide*; DMSO, Dimethyl sulfoxide; EPR, Electron paramagnetic resonance; ESP, Electrostatic potential map; ESR, Electron spin resonance; FRET, Fluorescence resonance energy transfer; FTIR, Fourier-transformed infrared; GLOB, Globulin; GLU, Glucose; HBA, Hydrogen bond acceptors; HMBC, Heteronuclear multiple bond correlation; HMQC, Heteronuclear multiple quantum coherence; HOMO, Highest occupied molecular orbital; HPLC, High performance liquid chromatography; IRS1, Insulin receptor substrate 1; LC/MS, Liquid chromatography–mass spectrometry; LC/Q-TOF, Liquid Chromatography Quadrupole Time-of-Flight; LUMO, Lowest unoccupied molecular orbital; MALDI TOF/TOF MS, Matrix Assisted Laser Desorption Ionization-Time of Flight Mass Spectrometry; MeCN, Acetonitrile; MeOH, Methanol; NMR, Nuclear magnetic resonance; ORTEP, Oak ridge thermal ellipsoid plot; P-gp, P-glycoprotein; PI3 (PDE), Phosphatidylinositol 3 kinase; PTP1B, Protein tyrosine phosphatase; TP, Total proteins; Trp, Tryptophan.

* Corresponding author at: Laboratory for Inorganic and Bioinorganic Chemistry, Department of Chemistry Faculty of Science, University of Sarajevo, Zmaja od Bosne 35, 71000 Sarajevo, Bosnia and Herzegovina.
E-mail address: adnan.zahirovic@pmf.unsa.ba (A. Zahirović).

https://doi.org/10.1016/j.jinorgbio.2023.112232
Received 7 February 2023; Received in revised form 6 April 2023; Accepted 14 April 2023
Available online 15 April 2023

last 30 years due to their promising antidiabetic activity.

The antidiabetic potential of vanadium compounds is well documented and a wide range of compounds, including simple salts and its coordination complexes, had been tested for insulin-mimicking activity in streptozotocin-induced diabetic Wistar rats [1–4]. Several compounds, including $VOSO_4$ [5] and [VO(etylmaltolato)$_2$] [6] have completed phase I and phase II of clinical trials. Although the exact mechanism by which metal ions and complexes act as insulin mimics is still unknown, it seems that redox processes must be critical elements for the biological activity of vanadium compounds, since vanadium complexes differing only in oxidation state have diverse biological features [7]. Indeed, there is evidence that insulin receptors are activated by inhibiting protein tyrosine phosphatase (PTP1B), which is connected to the activation of cytosolic nonreceptor tyrosine kinase, direct phosphorylation of insulin receptor substrate 1 (IRS1) and activation of phosphatidylinositol 3 kinase (PI3 (PDE)) [8,9].

From the structural point of view $V^{IV}O$ moiety is important in designing new insulin-mimicking agents since most of the complexes showing good antidiabetic activity contain this structural feature [10]. Moreover, it seems that regardless on oxidation state of vanadium complex administered *in vivo* $V^{IV}O$ specie is likely the form transported in blood as the most stable form in reducing biological environments [11]. On the other hand, hydrazones are versatile class of stereochemically flexible organic ligands which ligate metals mostly as bidentate or tridentate neutral, monoanionic or dianionic ligands in keto-amine or enol-imine form [12]. Additionally, diverse possibilities of controlling the donor atoms of hydrazone ligands provide synthetic routes to complexes with attractive structural, magnetic, electrochemical, catalytic or biological properties in which structure – activity relationships can be meaningfully established [13].

Given that the activity, distribution, metabolism and excretion of drugs is significantly affected by binding to albumin as the most abundant plasma protein, investigation of the interaction of new compounds with albumin is one of the first steps in the biological evaluation of new compounds [14]. It was empirically established that large binding constant of drugs with proteins leads to strong, most often irreversible binding, which sometimes results in drugs being inactivated before reaching their molecular target [15–18]. Certainly, the exceptions are compounds whose intentional binding to a protein increases their bioactivity. In this contest, preparing the vanadium complexes having a moderate affinity toward albumin, would give good drug candidates.

Here, we report the synthesis and full characterization of five novel heteroleptic oxidovanadium(IV) complexes of salicylaldehyde-based 2-furoic acid hydrazones, along with the promising *in vivo* antidiabetic activity of nitro derivative. Furthermore, the mild hypoalbuminemia observed *in vivo* motivated the study of complex – albumin interaction *in vitro* to gather the insight into the nature of binding.

2. Experimental

2.1. Chemicals

All chemicals used for syntheses, spectroscopic characterization, and interaction with BSA were of analytical grade unless otherwise stated. Vanadyl acetylacetonate was prepared by the reported procedure [19]. Lyophilized powder of bovine serum albumin (BSA, ≥98%) was acquired from Sigma Aldrich. Dimethylsulfoxide was dried over molecular sieves (3 Å). Streptozotocin (≥75% α-anomer basis, ≥98% (HPLC), powder, Sigma Aldrich), ketamine (Intervet International, Boxmeer, The Netherlands,) and diazepam (Alkaloid, Skopje, North Macedonia) were used as received.

2.2. Physical measurements

Elemental analyses were performed on a Perkin Elmer 2400 Series II CHNS analyzer. Mass spectra were collected on a 4800 Plus MALDI TOF/TOF analyzer in positive ion reflector mode using the α-cyano-4-hydroxycinnamic acid matrix. All NMR spectra of the ligands were recorded using a Bruker AV300 spectrometer operating at 300.130 MHz for ^{1}H and 75.475 MHz for ^{13}C. The spectra were measured at 25 °C from DMSO-d_6 which signals at 2.50 ppm, and 39.51 ppm were used as references for the recorded ^{1}H and ^{13}C spectra, respectively. Individual ligand resonances were assigned based on their chemical shifts, multiplicities, integrals, and cross peaks in the recorded 2D NMR spectra: ^{1}H—^{1}H COSY (Correlation Spectroscopy), ^{1}H—^{13}C HMQC (Heteronuclear Multiple Quantum Coherence) and ^{1}H—^{13}C HMBC (Heteronuclear Multiple Bond Correlation). Fourier-transformed infrared spectra were collected in transmission mode using KBr pellet technique on a Perkin Elmer BX FTIR. Electronic spectra of the complexes and ligands were recorded in MeOH (5×10^{-5} M) using a Perkin Elmer Bio-Lambda 35 in the range 200–1100 nm. Fluorimetric measurements were done on a PerkinElmer LS55 Luminescence. Bruker Elexsys 580 FT/CW spectrometer was used for X-band ESR measurements. The measurements were performed at liquid nitrogen temperature, 78 K, and at room temperature, 295 K. For all measurements, the modulation frequency was 100 kHz and the magnetic field modulation amplitude was 0.5 mT. The microwave frequency was 9.71 (1) GHz at 78 K and 9.63 (1) GHz at room temperature. Cyclic voltammograms were recorded in dichloromethane solution (1×10^{-3} M) using 0.1 M tetrabutylammonium hexafluorophosphate as the supporting electrolyte and a three-electrode system with Pt-wire as the counter and working electrode and Ag/AgCl as a reference electrode connected to the working solution over a salt bridge. All measurements were done on a BioLogic SP-300 potentiostat. Conductometry measurements were performed in DMSO solution (1×10^{-3} M) using a Phywe conductometer. The hydrolytic behavior of complexes in aqueous solution was investigated in MeCN:H_2O (1:1, *v*/v) using mass spectrometry. Data were acquired and analyzed using MassHunter LC/MS Data Acquisition Software version 10 for data collection from the 6546 LC/Q-TOF (Agilent, USA).

2.3. X-ray crystallography

Data collection was performed at room temperature on an XtaLAB Synergy diffractometer with the micro-focus sealed X-ray tube (λ = 1.54183 Å). Data reduction and cell refinement were carried out using the CrysAlisPro (Version 1.171.42.62a, Rigaku, 2020), and standard multi-scan absorption correction was applied. Structures were solved by direct methods with SHELXT [20] and refined by a full matrix least-squares refinement based on F2, with SHELXL [21]. Molecular illustrations were prepared with MERCURY [22]. Calculations of molecular geometries and crystal packing parameters were performed with PLATON [23]. All software for data solution refinement and illustration is included in the WinGX package [24]. Hydrogen atoms were included in their geometrically calculated positions and refined according to the riding model.

2.4. Syntheses of hydrazone ligands, H_2L^1 – H_2L^5

The ligands were prepared by the condensation reaction of 2-furoic acid hydrazide (10 mmol) with salicylaldehyde or a 5-substituted derivative of salicylaldehyde (10 mmol) in ethanol (70 mL) under reflux for 3 h as previously reported [25]. The volume of ethanol was reduced to half under the vacuum and the corresponding hydrazone ligands was obtained by cooling. The yields are above 70% in all cases.

2.5. Syntheses of vanadium(IV) complexes [VO(bpy)(L)], (**1**)–(**5**)

The solution or suspension of appropriate hydrazone ligand H_2L^1 – H_2L^5 (0.5 mmol) and 2,2′-bipyridine (0.5 mmol, 78 mg) in methanol (30 mL) was added to a well-stirred solution of vanadyl acetylacetonate (0.5 mmol, 133 mg) in methanol (10 mL) and the resulting mixture was stirred overnight. The gravitational filtration afforded vanadium(IV)

complexes (**1**)–(**5**) as red-orange powders, which were thoroughly washed with cold methanol and dried under a vacuum.

(2,2′-bipyridine-κ^2*N*,*N*′)[(2*Z*,*N*′*E*)-*N*′-2-oxido-κ*O*-benzylidenefuran-2-carbohydrazonato-κ^2*N*,*O*(2-)]oxidovanadium(IV), (**1**). Red-brown powder. Yield: 166 mg (74%). *Anal. Calc*. (%) for $C_{22}H_{16}N_4O_4V$ (*Mr* = 451.33): C, 58.55; H, 3.57; N, 12.41. *Found* (%): C, 58.57; H, 3.65; N, 12.48. MS for $[C_{22}H_{16}ClN_4O_4V]^+$ *Found* (*Calc*.): 452.0684 (452.0689). IR (KBr) ν (cm^{-1}): 1612 ν(C=N_{hyd}N), 1510 ν(C=NN_{hyd}), 1349 ν(C − O_{enol}), 761 δ_{oop}(bpy), 964 ν(V=O). UV/Vis (MeOH) λ_{LMCT} / nm (log ε): 393 (3.74).

(2,2′-bipyridine-κ^2*N*,*N*′)[(2*Z*,*N*′*E*)-*N*′-5-chloro-2-oxido-κ*O*-benzylidenefuran-2-carbohydrazonato-κ^2*N*,*O*(2-)]oxidovanadium(IV), (**2**). Red-brown powder. Yield: 198 mg (82%). *Anal. Calc*. (%) for $C_{22}H_{15}ClN_4O_4V$ (*Mr* = 485.77): C, 54.39; H, 3.11; N, 11.53. *Found* (%): C, 53.69; H, 3.38; N, 11.24. MS for $[C_{22}H_{16}ClN_4O_4V]^+$ *Found* (*Calc*.): 486.0285 (486.0300). IR (KBr) ν (cm^{-1}): 1610 ν(C=N_{hyd}N), 1513 ν(C=NN_{hyd}), 1350 ν(C − O_{enol}), 768 δ_{oop}(bpy), 964 ν(V=O). UV/Vis (MeOH) λ_{LMCT} / nm (log ε): 409 (3.86).

(2,2′-bipyridine-κ^2*N*,*N*′)[(2*Z*,*N*′*E*)-*N*′-5-bromo-2-oxido-κ*O*-benzylidenefuran-2-carbohydrazonato-κ^2*N*,*O*(2-)]oxidovanadium(IV), (**3**). Red-brown powder. Yield: 217 mg (82%). *Anal. Calc*. (%) for $C_{22}H_{15}BrN_4O_4V$ (*Mr* = 530.22): C, 49.83; H, 2.85; N, 10.57. *Found* (%): C, 49.64; H, 2.84; N, 10.56. MS for $[C_{22}H_{16}ClN_4O_4V]^+$ *Found* (*Calc*.): 529.9814 (529.9794). IR (KBr) ν (cm^{-1}): 1606 ν(C=N_{hyd}N), 1511 ν(C=NN_{hyd}), 1350 ν(C − O_{enol}), 774 δ_{oop}(bpy), 956 ν(V=O). UV/Vis (MeOH) λ_{LMCT} / nm (log ε): 409 (3.91).

(2,2′-bipyridine-κ^2*N*,*N*′)[(2*Z*,*N*′*E*)-*N*′-5-nitro-2-oxido-κ*O*-benzylidenefuran-2-carbohydrazonato-κ^2*N*,*O*(2-)]oxidovanadium(IV), (**4**). Red-brown powder. Yield: 193 mg (78%). *Anal. Calc*. (%) for $C_{22}H_{15}N_5O_6V$ (*Mr* = 496.33): C, 53.24; H, 3.05; N, 14.11. *Found* (%): C, 52.71; H, 2.90; N, 14.00. MS for $[C_{22}H_{16}N_5O_6V]^+$ *Found* (*Calc*.): 497.0551 (497.0540). IR (KBr) ν (cm^{-1}): 1607 ν(C=N_{hyd}N), 1506 ν(C=NN_{hyd}), 1355 ν(C − O_{enol}), 762 δ_{oop}(bpy), 971 ν(V=O). UV/Vis (MeOH) λ_{LMCT} / nm (log ε): 382 (4.17).

(2,2′-bipyridine-κ^2*N*,*N*′)[(2*Z*,*N*′*E*)-*N*′-5-hydroxo-2-oxido-κ*O*-benzylidenefuran-2-carbohydrazonato-κ^2*N*,*O*(2-)]oxidovanadium(IV) monohydrate, (**5**). Red-brown powder. Yield: 144 mg (62%). *Anal. Calc*. (%) for $C_{22}H_{18}N_4O_6V$ (*Mr* = 485.34): C, 54.44; H, 3.74; N, 11.54. *Found* (%): C, 54.58; H, 3.81; N, 11.69. MS for $[C_{22}H_{16}N_4O_5V]^+$ *Found* (*Calc*.): 468.0629 (468.0639). IR (KBr) ν (cm^{-1}): 1605 ν(C=N_{hyd}N), 1512 ν(C=NN_{hyd}), 1381 ν(C − O_{enol}), 767 δ_{oop}(bpy), 963 ν(V=O). UV/Vis (MeOH) λ_{LMCT} / nm: 433.

2.6. Quantum chemical calculations

Quantum chemical calculations were done at B3LYP and M06-2× [26,27] levels with 6–31++g(d,p) basis set using Gaussian09 RevD.01 and GaussView 6.0 [28,29]. The quantum chemical parameters of interest were calculated as described elsewhere [30–32]. The ADME (Absorption, Distribution, Metabolism, and Excretion) analysis was then performed using SwissADME to predict the effects and responses of vanadium complexes in human metabolism [33].

2.7. In vivo study

Fifteen healthy male Wistar rats, weighing between 190 and 210 g, were used for *in vivo* experiments. The rats were housed in separate cages under regular laboratory conditions and fed by Oxbow's Essentials-Adult food and water *ad libitum*. The animals were separated into three experimental groups. The control group (n = 5) received an intraperitoneal injection of citrate buffer (pH 4.5; 0.1 M). The second group (n = 5) received a single intraperitoneal injection of streptozotocin (35 mg/kg in 1 mL of citrate buffer) and rats with blood glucose levels above 11.11 mmol/L were considered for analysis. The second group was further orally administered oxidovanadium(IV) complex (**4**) (15 mg/kg DMSO:water 1:1 *v*/v, 1 mL) daily for one week. The third group (n = 5) was treated the same as the second group only by vanadium complex (**4**). All animals were sacrificed on the eighth day of the experiment by an intraperitoneal mixture of ketamine and diazepam (60 mg/kg and 7 mg/kg, respectively). The blood samples (3 mL) were obtained by cardiac puncture and centrifuged to obtain serum for the biochemical analysis. Biochemical parameters (urea (BUN), creatinine, total proteins (TP), and albumins (ALB)) were analyzed by biochemical analyzer (Mindray, BS-200, China). The difference between total proteins and albumins was extrapolated to represent the globulin (GLOB) level. Glucose (GLU) value measurements were obtained after the third (from tail vein) and seventh day of the experiment using a glucometer (AccuCheck, Roche, Switzerland). The statistical analysis was carried out using SPSS 20.0. The mean and standard deviations were used to summarize quantitative variables. One-way ANOVA was used to assess normally distributed continuous variables, and the least significant difference test was used *post hoc* to identify individual group differences. $P < 0.05$ was regarded as a statistically significant difference in all analyses. Animal handling, care, and treatment were all required throughout the experimental phase. In Bosnia and Herzegovina, experiments involving animals are subject to the Law on the Protection and Welfare of Animals (Official Gazette of BiH, Nos. 25/2009 and 9/2018). The animals were also taken care of per the "Declaration on Animal Rights," and "Universal Declaration on Animal Welfare".

2.8. Interaction with BSA

The interaction of compounds with BSA was investigated in 10 mM Tris-HCl buffer solution by spectrofluorimetric titration of BSA with complexes. The working solution of BSA was prepared by dissolving BSA in 10 mM Tris-HCl buffer until 1 μM solution was obtained. The concentration of BSA was determined by electron spectroscopy based on the extinction coefficient of 43,824 M^{-1} cm^{-1} at 280 nm. The stock solutions of complexes were prepared in methanol (1×10^{-4} M). Spectrofluorimetric titration was carried out by titrating a solution of BSA (2000 μL, 1 μM) with 10-μL amounts of complex and recording the emission spectra in 290–420 nm range with 278 nm as excitation wavelength. Synchronous emission spectra were collected similarly as mentioned above only in 250–310 nm range with $\Delta\lambda$ = 15 nm and $\Delta\lambda$ = 60 nm.

3. Results and discussion

3.1. Syntheses

The condensation of 2-furoic acid hydrazide with salicylaldehyde and its 5-substituted derivatives (Scheme 1) afforded tridentate hydrazone ligands H_2L^1 – H_2L^5 which were identified by ^{1}H and ^{13}C NMR spectra (Figs. S9 − S14) and infrared and electronic spectra.

Five novel heteroleptic vanadium(IV) complexes (**1**)–(**5**) with the general composition [VO(bpy)(L)], where L is a dibasic tridentate hydrazone ligand, were prepared by solution synthesis reacting the equimolar amounts of vanadyl acetylacetonate with the hydrazone ligands H_2L^1 – H_2L^5 and 2,2′-bipyridine in methanol (Scheme 2).

Coordination of hydrazone ligands as a tridentate dianionic ligand to V(IV) was assured by deprotonation with the acetylacetonate anion from starting $VO(acac)_2$ which acts as a base. Stabilization of vanadium(IV) in the resulting VO_3N coordination environment toward easy aerial oxidation to V(V) was achieved using 2,2′-bipyridine as the π-acceptor coligand. Thorough washing of the complexes with methanol is needed to remove all acetylacetone. The resulting orange-red oxidovanadium (IV) complexes (**1**)–(**5**) are readily soluble in DMSO, DMF, CH_2Cl_2, $CHCl_3$, and MeCN, moderately soluble in lower alcohols, acetone, benzene and toluene, very slightly soluble in water and practically insoluble in ether.

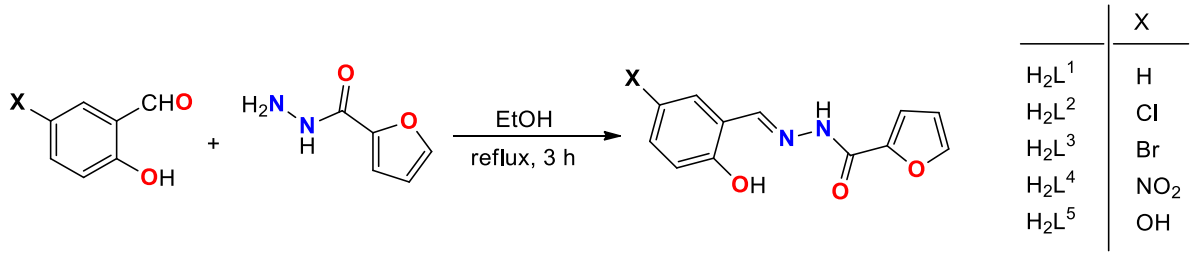

Scheme 1. Synthesis of hydrazone ligands H_2L^1 – H_2L^5.

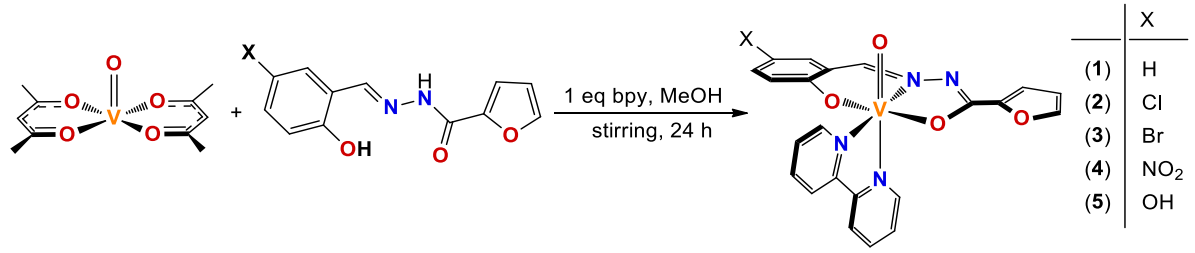

Scheme 2. Synthesis of vanadium(IV) hydrazone complexes (**1**)–(**5**).

3.2. Molecular and crystal structure

The single crystal of complex (**2**) was obtained by slow diffusion of hexane in a dichloromethane solution of (**2**) for several days. The crystal data, data collection and refinement parameters are summarized in Table 1. Complex (**2**) crystallizes in *C2/c* monoclinic space group with eight molecules per unit cell. Vanadium is 6-coordinated in a form of a distorted tetragonal bipyramid with O32 and N20 at the apical positions, shortened and elongated, respectively (Fig. 1, Table 1). The hydrazone ligand coordinates the vanadium(IV) in tridentate dianionic fashion through imine nitrogen and enol and carbonyl oxygen atoms. The bipyridine is orthogonally positioned to the hydrazone ligands occupying two coordination positions. The terminal oxygen atom occupies the sixth coordination position. There are no classic H-bonds in the structure. The coordination sphere angles and bond distances are given in Table 2.

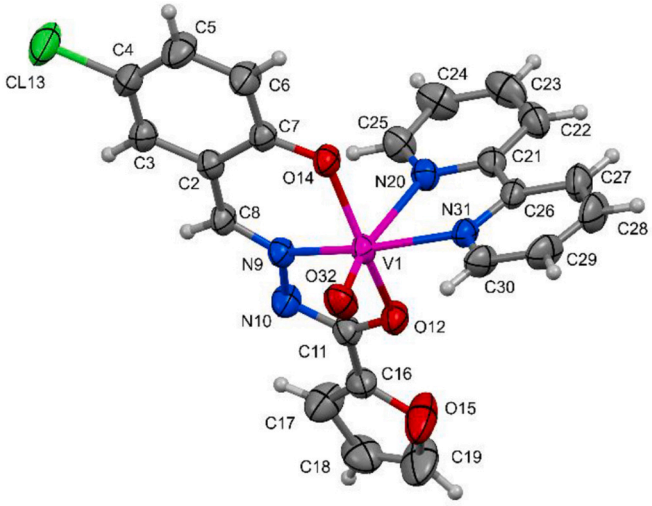

Fig. 1. ORTEP representation of the molecular structure of (**2**). Thermal ellipsoids are given at the 50% probability level.

Table 1
Crystallographic data for (**2**).

Structure	(**2**)
Brutto form.	$C_{22}H_{15}N_4O_4VCl$
M_r (gmol^{-1})	485.77
Crystal color and habit	Red plate
Cryst. (mm)	0.05 × 0.09 × 0.20
F(000)	1976
μ(mm^{-1})	5.504
Space group	*C2/c*
a (Å)	21.0083 (3)
b (Å)	8.2109 (2)
(Å)	25.3940 (5)
$\alpha = \gamma$ (°)	90.
β (°)	108.147 (2)
V (Å^3)	4162.5 (2)
Z	8
R_{int}	0.041
R_σ	0.056
θ max (°)	79.68
Unique	4402
Obs.[$I > 2\sigma(I)$]	3912
Parameters	289
R_1 [$I > 2\sigma(I)$]	0.040
wR_2, all	0.112
S	1.053
ρ_{max},ρ_{min}(eÅ^{-3})	0.32, −0.51

Table 2
Coordination sphere geometry around V in (**2**).

Distances	Å	Angles	°
V1 O32	1.6024 (16)	O32 V1 O14	102.01 (8)
V1 O14	1.9493 (14)	O32 V1 O12	99.95 (7)
V1 O12	2.0148 (14)	O32 V1 N9	103.17 (7)
V1 N9	2.0488 (13)	O32 V1 N31	92.69 (7)
V1 N31	2.1555 (14)	O14 V1 N20	81.06 (6)
V1 N20	2.2996 (17)	O12 V1 N20	80.90 (6)
		N9 V1 N20	92.48 (6)
		N31 V1 N20	71.50 (6)
		O14 V1 N9	87.56 (6)
		O14 V1 N31	94.05 (5)
		O14 V1 O12	155.31 (6)
		O12 V1 N9	76.54 (6)
		O12 V1 N31	96.05 (6)
		N9 V1 N31	163.39 (7)
		O32 V1 N20	164.12 (6)

3.3. Chemical and spectroscopic characterization

CHN analysis confirmed the purity and composition of heteroleptic oxidovanadium(IV) hydrazone complexes (**1**)–(**5**). The vanadium monoisotopic distribution of molecular ion peak $[M + H]^+$, along with the anticipated molecular ion masses, were confirmed by mass spectrometry for all five complexes (Table S3 and Figs. S4 − S8). Coordination of hydrazones to vanadium(IV) as tridentate dianionic ligands through deprotonated phenolic oxygen, imine nitrogen, and deprotonated enol oxygen of enol-imine form of hydrazone ligand was confirmed by infrared spectroscopy (Table S1 and Figs. S1 − S2).

Infrared spectra of ligands indicate that in the solid state the salicylaldehyde furoic acid hydrazones are predominantly present in keto-amine form [34]. The bands corresponding to the stretching vibrations of the N − H (3112–3146 cm^{-1}) and C═O (1652–1671 cm^{-1}) bonds of the keto-amine form of the ligand were not found in the spectra of the corresponding vanadium complex (**1**)–(**5**). Though, the new bands corresponding to the newly formed imine group (1506–1513 cm^{-1}) and the C − O bond (1349–1381 cm^{-1}) of the deprotonated enol were found, confirming the coordination of the hydrazone ligands H_2L^1 – H_2L^5 to vanadium(IV) in the enol-imine form *via* deprotonated enol oxygen [35]. Coordination of the hydrazones through the imine nitrogen resulted in a shift of the C═N stretching vibration toward lower wavenumbers ($\Delta\nu$ = 7–26 cm^{-1}) in the spectra of the complexes (1612–1605 cm^{-1}) in comparison with the spectra of the native ligands (1633–1619 cm^{-1}) [36]. The stretching vibrations of the Ar − OH bond in the spectra of the ligands are positioned in the range 1260–1292 cm^{-1}, while in the spectra of the complexes they are shifted to higher wavenumbers ($\Delta\nu$ = 12–28 cm^{-1}), which is consistent with the coordination of the ligand through deprotonated phenolic oxygen [37,38]. The shift toward higher wavenumbers is a direct consequence of the C − O bond weakening due to the formation of a weaker *V* − O bond compared to the stronger O − H bond. The bands arising from out-of-plane and in-plane deformations of the bipyridine ring are found in the spectra of the vanadium complexes in the range 761–774 cm^{-1} and 651–662 cm^{-1}, respectively. The sectra of all five vanadium (**1**)–(**5**) complexes exhibit a sharp band of moderate intensity in 956–971 cm^{-1} region distinctive for *V*═O stretching [39].

Electronic spectra of vanadium complexes (**1**)–(**5**) are consistent with [VO(bpy)(L)] composition. A typical electronic spectrum is shown in Fig. 2, while other data can be found in Supplement (Table S2 and Fig. S3). As expected for electron-poor d^1 V(IV) complexes electronic spectra are dominated by ligand-centred transitions. In the deep ultraviolet region, two bands arising from joint aromatic π → π* transitions of hydrazone ligand and bipyridine, are found near 205 and 235 nm. The band near 280 nm is purely Gaussian in shape and its oscillator strength varies little with the change of hydrazone ligand hence indicating this band predominantly rises from n → π* transitions of coordinated bipyridine. The band in 321–340 nm region in spectra of complexes cannot be explicitly ascribed to certain transition since second-derivative spectroscopy reveals this band arises from at least two n → π* transitions of similar energies, probably involving electrons of imine nitrogen and deprotonated phenolic oxygen. The two most distinctive features of electronic spectra of hydrazonato oxidovanadium(IV) complexes (**1**)–(**5**) are positioned in the visible region of the spectrum. The band positioned in 382–433 nm region is highly dependent on hydrazone ligand and appears upon its coordination to V(IV). Based on its solvatochromic nature, varying position, and oscillator strength dependent on hydrazonato ligands, this band can be undoubtedly assigned to the charge transfer band. Considering low electron population of vanadium(IV) and an increased electron density on hydrazonato ligand due to the deprotonation compared to the free hydrazone, this transition can be ascribed to ligand-to-metal charge transfer [40]. The red region of the visible spectra gives rise to a well-defined low-energy shoulder band arising from Laporte-forbidden spin-allowed d-d transition consistent with d^1 configuration of V(IV) in a distorted octahedral environment [38,41].

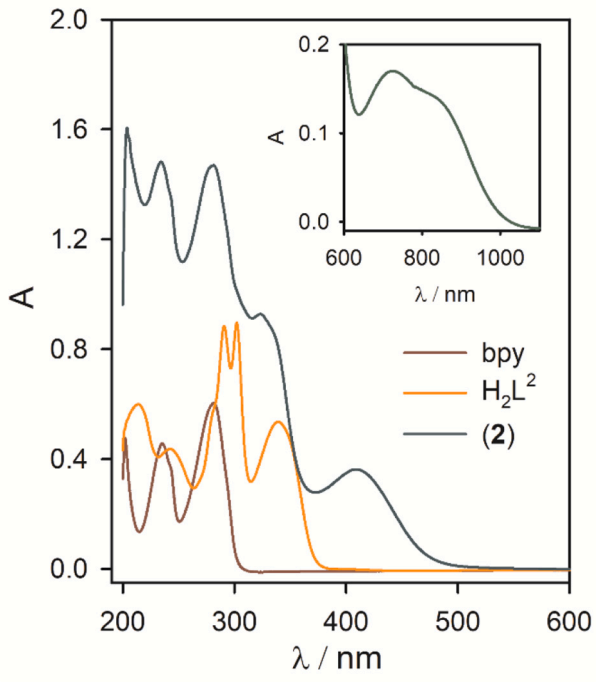

Fig. 2. Electronic spectra of ligands and corresponding vanadium(IV) complex (**2**) in methanol (5×10^{-5} M). *Inset*: Enlarged region of d-d transition of complex (**2**) in methanol (1×10^{-3} M).

The magnetic properties of five polycrystalline vanadium(IV) complexes (**1**)–(**5**) were investigated by X-band electron spin resonance/electron paramagnetic resonance (ESR/EPR) spectroscopy. The spectra obtained at room temperature (295 K) and liquid nitrogen temperature (78 K) are presented in Fig. 3. Spectral simulations were done using EasySpin software [42] with the reduced form of the spin-Hamiltonian for vanadium(IV) ions:

$$\mathbf{H} = \mu_B\, \mathbf{B}\cdot\mathbf{g}\cdot\mathbf{S} \qquad (1)$$

where μ_B is Bohr magneton constant, **g** is the **g**-tensor, **B** is the magnetic field vector and **S** is the electron spin operator.

The vanadium(IV) ion has an electron spin $S = 1/2$ and its stable isotope ^{51}V of nearly 100% natural abundance has nuclear spin $I = 7/2$ and thus eight hyperfine lines could be detected in ESR spectra [43]. The obtained ESR spectra of investigated oxidovanadium(IV) complexes (**1**)–(**5**) are assigned to vanadium (IV) ions (d^1 configuration) with spin $S = 1/2$. Hyperfine interactions between electron spin $S = 1/2$ and nuclear spins in oxidovanadium(IV) complexes (**1**)–(**5**) were not experimentally detected, indicating that hyperfine splitting was covered by the total spectral linewidth and the hyperfine term was omitted from the spin-Hamiltonian (1). The spectra were simulated assuming an anisotropic **g**-tensor and Lorentzian lineshape. In the spectral simulations, the same values of **g**-tensors were used at both investigated temperatures allowing linewidth l_w and **g**-strain values to change with temperature. The small variations in the local geometry of vanadium (IV) coordination can cause the distribution of g_x, g_y and g_z-values around some average values [44]. This effect described by $\mathbf{g}_{strain}$ parameters is also considered in the simulations. The spin-Hamiltonian values obtained from the simulations are given in Table 3.

The obtained results for the *g*-values for V(IV) ions are in agreement with the *g*-values from the literature [43,45,46]. The distance between the two nearest vanadium atoms in the crystal structure of the complex (**2**) is 6.946 Å. The V − V distances are large enough for significant exchange interactions to be observed in these compounds. In all investigated vanadium samples there is only one vanadium atom in the asymmetric unit, and we assume that in all five complexes there are

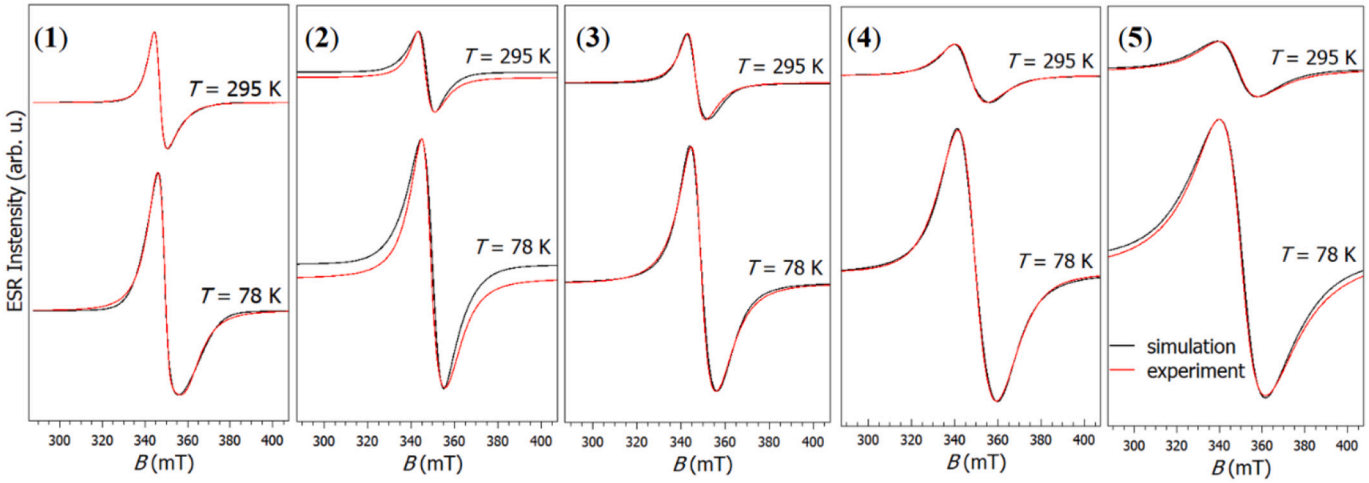

Fig. 3. Experimental (red lines) and simulated (black lines) ESR spectra of polycrystalline vanadium(IV) complexes (**1**)–(**5**) at 78 K and at 295 K. The ESR intensities of the spectra at different temperatures are presented in the real ratios. (For interpretation of the references to color in this figure legend, the reader is referred to the web version of this article.)

Table 3
The principal *g*-values of (**1**)–(**5**) complexes obtained from the spectral simulations given for two investigates temperatures, together with the parameters used for the simulations: $\mathbf{g}_{strain}$ and linewidths l_w.

Complex	$\mathbf{g} = [g_x\ g_y\ g_z]$	$\mathbf{g}_{strain}$	l_w (mT)	T (K)
(**1**)	[1.93 1.99 2.00]	[0.09 0.00 0.10] [0.14 0.01 0.04]	2.19 1.49	78 295
(**2**)	[1.98 1.98 1.98]	[0.03 0.40 0.16] [0.02 0.01 0.12]	5.17 3.99	78 295
(**3**)	[1.95 2.00 2.00]	[0.05 0.01 0.01] [0.05 0.01 0.00]	8.80 6.17	78 295
(**4**)	[1.93 2.01 2.01]	[0.04 0.38 0.03] [0.01 0.39 0.01]	12.64 11.40	78 295
(**5**)	[1.98 1.98 1.98]	[0.01 0.27 0.27] [0.01 0.39 0.19]	14.51 13.14	78 295

similar distances between the nearest vanadium atoms as in (**2**).

The redox properties of oxidovanadium(IV) hydrazone complexes (**1**)–(**5**) were investigated in dichloromethane using cyclic voltammetry. Electrochemical measurements show that oxidovanadium(IV) complexes (**1**)–(**5**) undergo three distinct redox processes in −2.0 to +1.0 V *vs* Ag/AgCl potential region (Fig. 4 and Figs. S15 − S18). All three redox processes are quasi-reversible with $\Delta E > 59$ m*V* and $i_{pa}/i_{pc} \neq 1$ which is consistent with the electrochemical behavior of similar vanadium complexes [47–50]. The redox process occurring at most positive potential values (+0.68 to +0.96 V), with well-defined anodic and cathodic peaks, arises from V^V/V^{IV} couple. The anodic peak of this couple appears regularly in the forward scan when going from low to higher potentials. In the reverse scan of the same cycle the cationic peak, corresponding to the reduction of V^V/V^{IV} appears but is absent in the forward scan if +1.0 V is taken as the starting potential. This is consistent with the fact that *V*(V) is only electrochemically generated and not

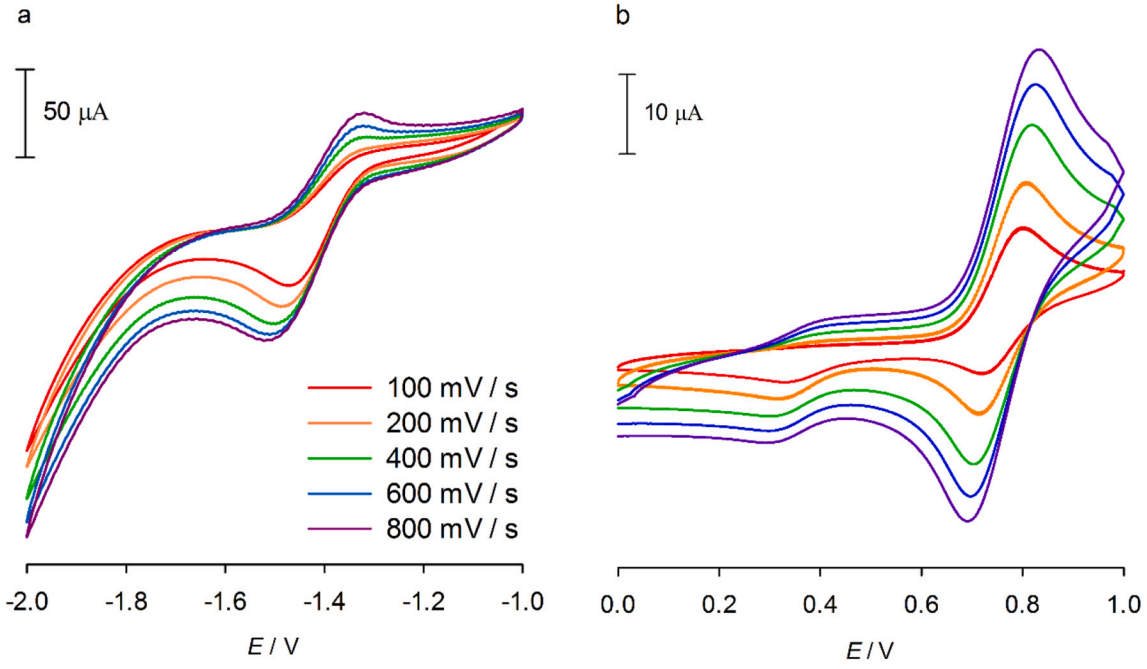

Fig. 4. Cyclic voltammograms of (**1**) (1×10^{-3} M) in dichloromethane solution of Bu_4NPF_6 (50 mM) at Pt electrode in: a) negative potential region; b) positive potential region at different scan rates.

present in an authentically formulated complex. The half-wave potential ($E_{1/2}$) of V^{V}/V^{IV} couple in complexes (**1**)–(**5**) is strongly dependent on the hydrazone ligand *i.e.* substituent in position 5 on salicylaldehyde component of furoic acid hydrazone affects stabilization of V(IV) oxidation state. The lowest $E_{1/2}$ value was observed for complex (**5**) having an electron-donating hydroxyl substituent. The most positive half-wave potential value was observed for complex bearing electron-withdrawing nitro substituent implying the most stable *V*(IV) oxidation state is in complex (**4**). The cathodic and anodic peak currents of this redox process are linearly related to the square root of the scan rate ($R^2 \geq 0.99$) indicating diffusion-controlled process [51].

The redox process arising at slightly lower potentials ($E_{1/2} = +0.35$ to $+0.59$ *V*) can be attributed to the V^{IV}/V^{III} redox couple. For complex (**5**) this redox process was not observed. Only at high scan rates slight inflexion, corresponding to cathodic wave, can be seen near $+0.1$ *V*. The anodic peak of $V^{III} \rightarrow V^{IV} + e$ process in cyclic voltammograms of (**1**)–(**4**) is not observed at low scan rates, implying the chemical oxidation of electrochemically generated V^{III} is fast. At higher scan rates this peak appears and the peak separation values for complexes (**1**)–(**4**) are in the 80 and 102 mV range, still being larger than the theoretically expected 59 mV for a one-electron reversible process. In the strongly negative potential region a quasi-reversible redox process, with a half-wave potential value dependent on the hydrazone ligand ($E_{1/2} = -1.4$ to -1.8 V), was observed. Vanadium(IV) complexes having bipyridine or phenanthroline coligands are susceptible to a reversible one-electron reduction of the diimine ligand in this potential region [47,52]. However, taking into account that: (i) the process is not reversible, (ii) the half-wave potential is dependent on hydrazone ligand and (iii) the peak separation is very large ($\Delta E = 163$–494 mV), this process probably involves $V^{III} \rightarrow V^{II}$ reduction. Still simultaneous bpy → bpy^{-} reduction cannot be excluded *a priori* [53].

The values of molar conductance of 1 mM DMSO solutions of complexes (18–26 μS cm^2 mol^{-1}) are consistent with their non-electrolyte nature of oxidovanadium(IV) complexes (**1**)–(**5**).

3.4. Quantum chemical calculations

3.4.1. Molecular structure optimization

The importance of theoretical calculations in metal-based drug design arises from possibilities to efficiently investigate, find and compare activities of metal complexes, to detect their active sites important in biomolecular targeting and thus to predictably increase their activity. In this context, many properties of metal complexes can be studied and investigated using quantum chemical calculations. One of the most important factors determining the activities of metal complexes is electron density. High electron density regions of metal complexes interact with biomolecular targets by donating the electrons, while low-density regions can accept electron density from a biomolecular electron donors. Two important parameters that quantitatively describe these interactions are the HOMO and LUMO parameters of metal complexes. The calculated HOMO and LUMO parameters for vanadium complexes (**1**)–(**5**) are given in Table S5. The highest HOMO energy value among vanadium(IV) hydrazone complexes (**1**)–(**5**) was found for complex (**5**) with a 5-hydroxy substituent on salicylaldehyde part of hydrazone ligand indicating the strongest electron donating properties of (**5**) among the tested complexes [54]. On the other hand, the lowest LUMO energy values was obtained for complex (**4**) featuring 5-nitro substituent confirming the best electron-accepting abilities of the molecule [55]. The energy gap parameter ($\Delta E = E_{LUMO} - E_{HOMO}$) and electronegativity had the lowest value for complex (**5**) indicating that complex (**5**) could have the highest activity among vanadium(IV) hydrazone complexes (**1**)–(**5**), according to Gaussian calculations. The visual representation of HOMO and LUMO, along with the electrostatic potential map (ESP) is given in Fig. 5 for complex (**5**), while for other complexes can be found in ESI (Fig. S32). The red-colored regions in the ESP map, which are generally the regions where heteroatoms are found, are electron-rich, while the blue-colored regions are electron-depleted.

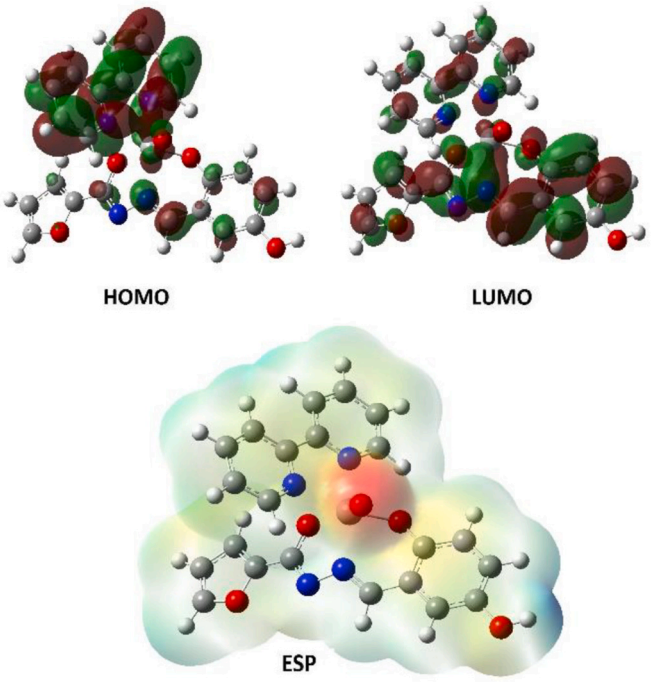

Fig. 5. HOMO, LUMO and ESP of complex (**5**).

3.4.2. Swiss-ADME analysis

Swiss-ADME analysis was performed to examine the ADME (absorption, distribution, metabolism, and excretion) properties of the vanadium(IV) hydrazone complexes (**1**)–(**5**). Six physicochemical indexes responsible for the bioavailability of the drug including lipophilicity, size, polarity, solubility, saturation, and flexibility are shown for each complex in Fig. 6. All six properties appear to be better for complex (**4**) compared to other vanadium(IV) hydrazone complexes.

More detail on ADME properties of vanadium complexes (**1**)–(**5**) is given in Table S6. Considering the Lipinski "Rule of Five", all five complexes have a number of hydrogen bond donors ≤5 (HBD = 1) and a number of hydrogen bond acceptors ≤10 (HBA = 4–6) [56]. The partition coefficient factor between octanol and water ($LogP_{o/w}$) for tested vanadium(IV) hydrazone complexes is in 0.23 (for (**4**)) to 1.53 range (for (**3**)) thus meeting the lipophilicity criteria ($-0.4 \leq LogP_{o/w} \leq 5.6$) [57]. The values of molar refractivities (MR = 115–128) also fall within the allowed range ($40 \leq MR \leq 130$) [58]. The topological polar surface area (TPSA) for all five complexes is lower (71–117 $Å^2$) than the maximum limit of 140 $Å^2$ making them potential candidates for reasonable cell membrane penetration [59]. Complexes (**2**) and (**3**) are expected to be able to cross the blood-brain barrier, while blood-brain barrier permeability is not expected for (**1**), (**4**), and (**5**).

Apart from the abovementioned parameters, the investigation of the behavior of the studied vanadium complexes toward certain pharmacokinetic proteins such as P-glycoprotein (P-gp) and cytochromes P450 (CYP) is of great importance. The most important task of P-gp is to keep the central nervous system away from xenobiotics [60]. Additionally, this protein is secreted in some tumor cells and leads to drug-resistant cancers. All five vanadium complexes are suitable P-gp substrates. Furthermore, information on the interaction of complexes with cytochromes (CYP) is pharmacologically important, since this group of isoenzymes metabolically plays an important role in drug clearance. It has been suggested that CYP and P-gp may work together to metabolize small compounds synergistically to promote tissue and organism protection [61]. The vanadium(IV) complexes (**1**)–(**5**) are found to be

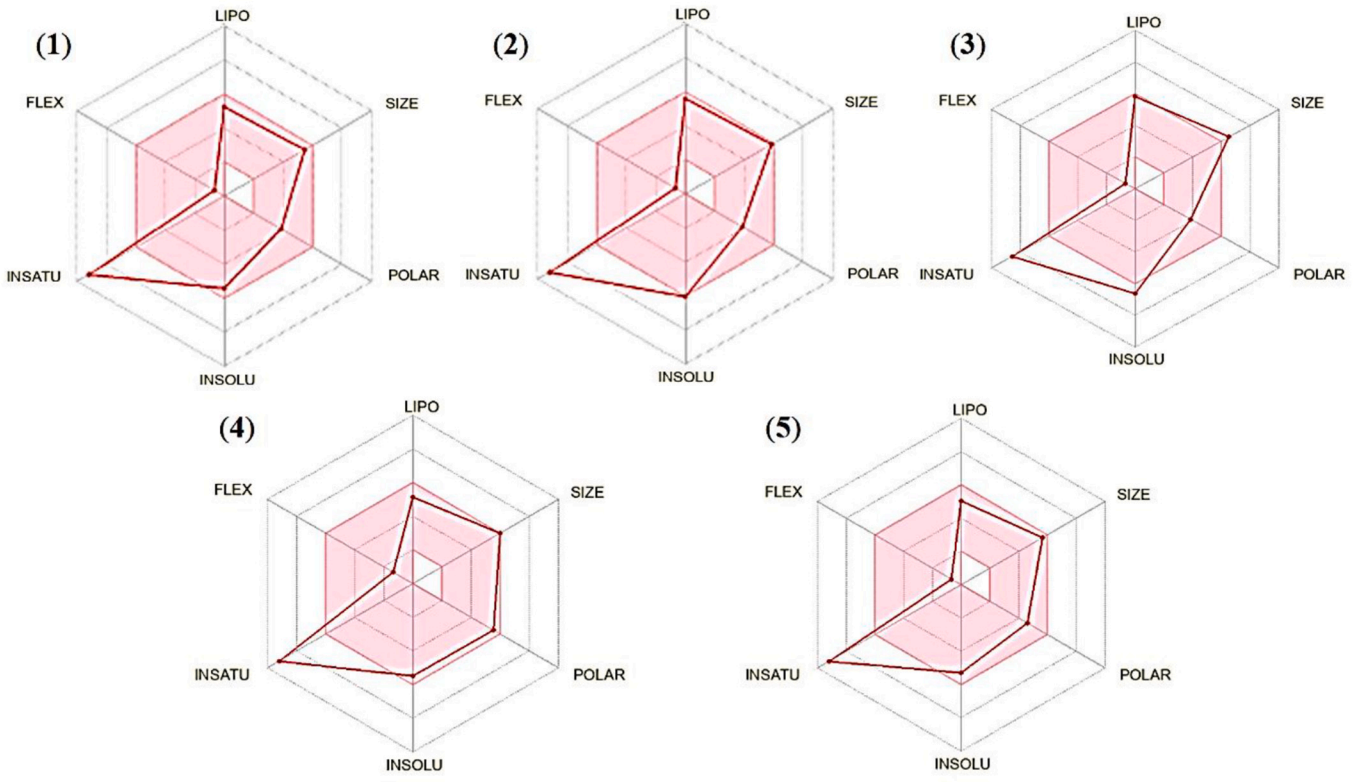

Fig. 6. Druglikness parameters for vanadium complexes (**1**)–(**5**).

CYP2C19 inhibitors.

In addition, the skin permeability coefficient (log *K*p), which is related to the size and lipophilicity of the metal complexes, is also given in Table S8. Based on the ADME analysis complex (**4**) is the best candidate for further biological evaluation.

3.5. *In vivo effects*

In vivo effects of oxidovanadium(IV) complex (**4**) on selected biochemical parameters of blood serum and its insulin-mimicking activity were tested on Wistar rats. Animals were divided into three experimental groups. The first group was a control group, the second group was streptozotocin-induced diabetic rats who were subjected to a daily oral dose of complex (**4**) for a week and the third group was

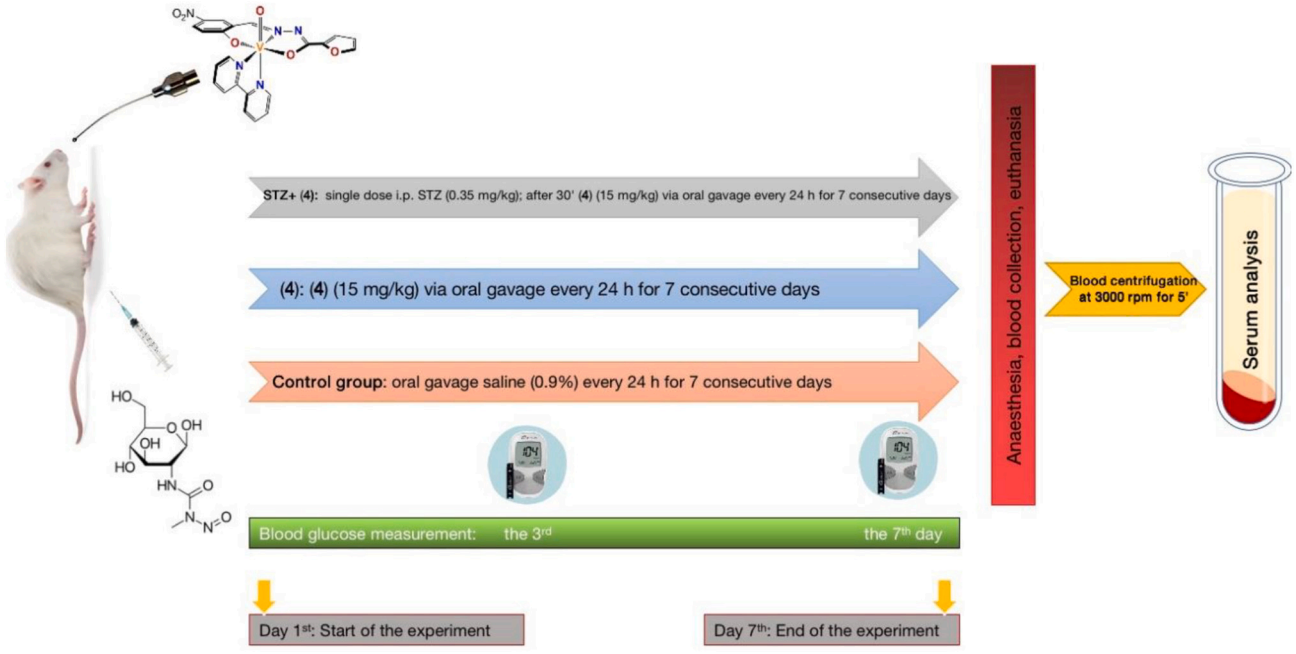

Fig. 7. The timeline and overview of the *in vivo* experiment.

healthy rats administered with a daily oral dose of complex (**4**) for a week. The timeline of the *in vivo* experiment is presented in Fig. 7.

The tested biochemical parameters are presented in Table 4. The significant decline of glucose levels on the seventh day in diabetic rats treated with complex (**4**) demonstrates the strong antidiabetic effect of this compound. However, administering vanadium complexes to diabetic animals can lead to certain harmful adverse effects, including gastrointestinal distress, slower weight gain, liver and renal toxicity [62]. We found that urea concentration is increased in both groups treated with complex (**4**) compared to the control group and is higher in healthy rats compared to diabetic rats. The increased blood urea levels are the consequence of renal failure, which in the case of vanadium compounds has been related to the production of free radicals and lipid peroxides which induce the destruction of cell membranes in kidneys [63].

The treatment of diabetic rats with (**4**) caused a decrease in creatinine and albumin concentrations compared to the control group and healthy rats treated only with complex (**4**). The observed hypoalbuminemia can be associated with severe impairments of the liver tissue. Globulin concentrations had significantly higher values in both groups of complex-treated rats compared to the control group. High globulin levels in diabetic rats treated with complex (**4**) indicate the potential existence of certain inflammation in the body, which could be related to streptozotocin application [64]. The promising result is that complex (**4**) partially regulates this inflammatory activity by inhibiting the activities of inflammatory cytokine and pro-inflammatory signaling as serum concentrations of globulins are lower in healthy rats treated with (**4**) compared to diabetic rats treated with (**4**).

Although complex (**4**) showed excellent insulin-mimetic ability it still has certain adverse effects, which are indirectly reflected in the concentration of albumin and urea in the blood. The observed moderate renal and hepatotoxicity warrant further investigation of organs impairments for chronic term application of (**4**).

3.6. Interaction with BSA

As the application of (**4**) leads to hypoalbuminemia in Wistar rats *in vivo* the interaction of vanadium complexes (**1**)–(**5**) with BSA was investigated *in vitro* to gather the insight into the nature of binding. Proteins, especially albumins, are considered the most probable extracellular biomolecular targets of drugs. The binding of metal complexes to proteins can affect complex metabolism, biotransformation and mechanism of action [65]. Moreover, absorption, distribution, toxicity, and biological activity of metal complexes are greatly affected by protein – complex interactions and thus they are one of the most important steps in the biological evaluation of potential drugs [66].

Table 4
Tested biochemical parameters in three groups of Wistar rats.

	First group		Second group		Third group	
Parameter	Control group		STZ + (**4**)		(**4**)	
Urea (mmol/L)	5.44 ± 0.36		6.36 ± 0.28 [a]		7.86 ± 0.39 [b]	
Creatinine (μmol/L)	63.17 ± 1.74		49.62 ± 3.72 [a]		52.55 ± 9.35 [b]	
Total proteins (g/L)	64.52 ± 4.18		64.80 ± 2.64		63.05 ± 2.14 [b]	
Albumins (g/L)	39. 52 ± 1.68		30.54 ± 0.72 [a]		30.61 ± 1.02 [b]	
Globulins (g/L)	24. 98 ± 3.82		34.26 ± 2.08 [a]		32.44 ± 1.23 [b]	
Glucose (mmol/l)	3rd day 4.66 ± 0.39	7th day 4.68 ± 0.44	3rd day 18.22 ± 0.79	7th day 6.48 ± 0.32	3rd day 4.90 ± 0.41	7th day 4.92 ± 0.31
P level (<0.05)	0.47		0.00 *		0.46	

[a] Significantly different between the first and second group of rats.
[b] Significant differences between the first and third group of rats.
* Significant differences between the 3rd and the 7th day.

The first step in the biological evaluation of new compounds is the examination of their behavior in aqueous solutions so that the activity could be reasonably attributed to a specific species existing in solution. Complexes that possess labile positions suitable for substitution with water molecules in aqueous solution experience aquatation or hydrolysis and those position are often responsible for covalent binding of complexes to biomolecular targets. The oxidovanadium(IV) complexes (**1**)–(**5**) have a coordinatively saturated V(IV) metal center enclosed with a terminal oxygen, a tridentate dianionic ONO donor hydrazone and a bidentate bipyridine. Based on the chemical reasons, it is not expected that substitution of the hydrazone ligand or bipyridine occurs in the aqueous solution [67], although in some cases bipyridine substitution cannot be excluded. Recently, several papers reported that substitution of bipyridine in oxidovanadium(IV) complexes can occur in aqueous solution [68,69], although the equilibrium is shifted to undissociated specie [69]. Therefore, the behavior of complexes (**1**)–(**5**) was investigated in aqueous solution using mass spectrometry. Mass spectra of complexes were recorded in acetonitrile/water mixture (1/1, *v*/v) and are shown in Figs. S19 − S23. Spectra clearly show that the substitution of bipyridine does not take place in aqueous solution for complexes (**1**)–(**5**) and aquatation product $[VO(L)(OH_2)_2]$ could not be identified. Moreover, products involving acetonitrile as ligand, $[VO(L)(NCMe)(OH_2)]$ and $[VO(L)(NCMe)_2]$,were not also observed. This is in accordance with the inertness of bipyridine for substitution from (**1**)–(**5**) which was also confirmed by electron spectroscopy. Thus, all biological activity can be attributed to authentically formulated oxidovanadium (IV) complexes (**1**)–(**5**).

Spectrofluorimetric titration of BSA with increasing concentrations of (bipyridine)(hydrazonato)oxidovanadium(IV) complexes (**1**)–(**5**) was employed to investigate albumin – complex interactions. When excited at 278 nm BSA shows strong fluorescence with an emission maximum near 340 nm owing to the intrinsic fluorescence of two tryptophan residues (Trp-134 and Trp-212). In presence of increasing concentrations of vanadium complexes BSA fluorescence is quenched as shown in Fig. 8a (Figs. S25–S32). The corresponding Stern-Volmer constants (K_{SV}) and binding constants (K_b) could be obtained graphically as described elsewhere [70] and are given in Table 5. The K_{SV} values are 10^5 M^{-1} and suggest there is a strong conformational change of BSA in presence of tested vanadium(IV) complexes. On the other hand, binding constants in (0.24–1.23) × 10^4 M^{-1} range indicate moderate reactivity of these compounds toward BSA. Complex (**2**) having chloro substituent at salicylaldehyde part of furoic acid hydrazone has the largest binding constant to BSA. The K_b values vary within 10-order magnitude with the change of the substituent on hydrazone ligand and decrease in order Cl > NO_2 > Br > OH > H.

The affinity of oxidovanadium(IV) complexes of furoic acid hydrazones (**1**)–(**5**) to BSA is lower compared to dioxidovanadium(V) salicylaldehyde-based hydrazone complexes [71] and neutral mononuclear oxidomethoxidovanadium(V) complexes of tridentate dibasic ONS Schiff base ligand derived from 2-hydroxy-5-(phenyldiazenyl)benzaldehyde and S-benzyldithiocarbazate [72] or oxidovanadium(V) complexes of oxaloyldihydrazones of salicylaldehyde and 2-hydroxy-1-naphthaldehyde [73]. Nevertheless, their BSA binding strength is comparable to mononuclear dioxidovanadium(V) complex $[VO_2L]$ of 2-acetylpyridine and salicylaldehyde hydrazones featuring 1-napthoyl, 2-furoyl and isonicotinoyl moieties [74] and binuclear $[(V^VO_2)_2(pedf)_2]$ complex where pedf is 2-acetylpyridine 2-furoic hydrazone [75].

The number of the binding sites of vanadium(IV) complexes with BSA is closer to 0.5 than 1, indicating no stoichiometric adducts of 1:1 composition are likely to be obtained, similar to the abovementioned $[(V^VO_2)_2(pedf)_2]$ complex [75]. The quenching rate constants (k_q) are in all cases larger than 10^{10} M^{-1} s^{-1} ((2.5–7.3) × 10^{13} M^{-1} s^{-1}) indicating that vanadium complexes (**1**)–(**5**) quench BSA fluorescence through static mechanism forming an adduct with BSA in ground state [76].

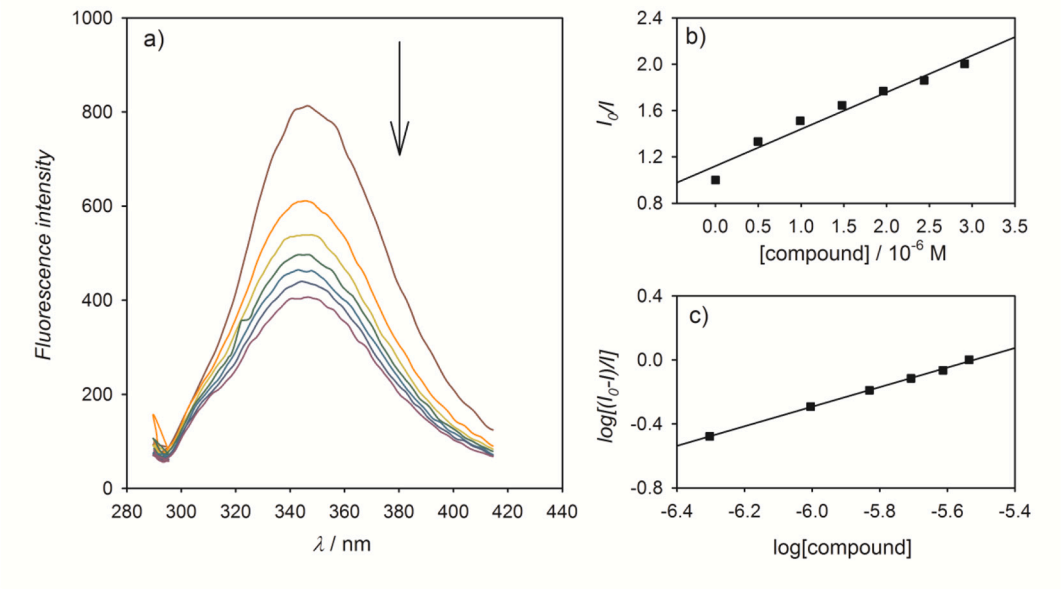

Fig. 8. Interaction of (**1**) with BSA in 10 mM Tris-HCl buffer pH 7.42: a) fluorescence quenching of BSA (1.10×10^{-6} M) in presence of an increasing concentration of (**1**); b) graphical determination of Stern-Volmer constant; b) graphical determination of binding constant and the number of binding sites.

Table 5
Data on the interaction of oxidovanadium(IV) hydrazone complexes (**1**)–(**5**) with BSA.

Complex	K_{SV} / M^{-1}	k_q / M^{-1} s^{-1}	K_b / M^{-1}	n	$\Delta\lambda^{15}_{max}$ / nm	$\Delta\lambda^{60}_{max}$ / nm
(**1**)	3.18×10^5	3.18×10^{13}	2.38×10^3	0.61	12	0.5
(**2**)	6.43×10^5	6.43×10^{13}	1.23×10^4	0.68	15	1
(**3**)	6.82×10^5	6.82×10^{13}	8.20×10^3	0.65	16	2
(**4**)	7.32×10^5	7.32×10^{13}	1.07×10^4	0.67	15	1
(**5**)	2.48×10^5	2.48×10^{13}	2.71×10^3	0.64	14	0

Further insight into the BSA – complex interactions can be gathered from synchronous fluorescence spectra which are highly sensitive to microenvironments of tryptophan or tyrosine, deepening on the fixed difference of emission and excitation wavelengths (Δλ) used for measurements. If the Δλ is fixed to 15 nm the information on the tyrosine microenvironment can be obtained, while the tryptophan microenvironment is investigated with Δλ = 60 nm [77].

The reasonable decrease of emission intensity in synchronous spectra (Fig. 9) suggests that the microenvironment of both, tyrosine and tryptophan, is affected by complexes (**1**)–(**5**) and that conformational change of protein is certain. While the emission intensity of the tryptophan fluorescence is significantly decreased no significant shifting of the peak maximum was observed (Table 5). On the contrary, substantial change in the position of the emission maximum of tyrosine was found for all five oxidovanadium(IV) complexes. The pronounced bathochromic shift (12–16 nm) indicates increased polarity *i.e.* less hydrophobic environment of tyrosine [78–80].

Forster resonance energy transfer (FRET) theory was used to evaluate the energy transfer between the fluorophore (BSA) and vanadium complexes (**1**)–(**5**). The overlap of the emission spectrum of the fluorophore and the vanadium complexes (**1**) is shown in Fig. 10 and was used to calculate an overlapping integral value (J). This further gave the values of critical distance between fluorophore and complex when the transfer efficiency is 50% (R_0) as described elsewhere [70]. The efficiency of the energy transfer (E) was calculated from the fluorescence intensities of BSA in the presence (I) and absence of complex (I_0) and further used to deduce the distance between the donor and acceptor at which energy transfer occurs (r).

The obtained values for all parameters (Table 6) are comparable to other rare examples of vanadium hydrazone complexes for which FRET analysis of BSA – complex interaction was done [72,81,82]. Considering the criteria $0.5\ R_0 < r < 1.5\ R_0$ is fulfilled, the values of the distance between donor and acceptor (r) in 2–8 nm range are diagnostic for a static mechanism of BSA fluorescence quenching and non-radiative energy transfer between oxidovanadium(IV) complexes (**1**)–(**5**) and BSA can be presumed.

Although spectrofluorimetric titrations at one temperature and FRET analysis can provide many data on the interaction of complexes with albumin, the nature of the forces involved in the interaction cannot be determined without thermodynamic data. The interaction of complex (**4**) with albumin was therefore examined at three temperatures in order to obtain data on Gibbs free energy and enthalpy and entropy change for the interaction. The van't Hoff plot for the interaction of complex (**4**) with BSA is shown in Fig. 11 and corresponding thermodynamic data presented in Table 7.

The criterion for consideration of the nature of the forces involved in the interaction of small molecules with albumin implies the simultaneous observation of the values of Gibbs free energy and enthalpy and entropy change. There are several experimentally proven ways of interaction of albumin with small molecules and they include [70,83,84]:

a) hydrophobic interaction ($\Delta G < 0$, $\Delta S > 0$, $\Delta H > 0$);
b) hydrogen bonding and van der Waals interactions ($\Delta G < 0$, $\Delta S < 0$, $\Delta H < 0$);
c) electrostatic interaction ($\Delta G < 0$, $\Delta S > 0$, $\Delta H \sim 0$);
d) immobilization ($\Delta G > 0$, $\Delta S < 0$, $\Delta H < 0$);
e) covalent binding ($\Delta H > 120$ kJ mol^{-1}).

The binding constant value for interaction of (**4**) with BSA decreases with a temperature increase indicating weakening of complex – BSA adduct at higher temperatures. Negative values of Gibbs free energy confirm that interaction between complex and BSA is spontaneous at all three temperatures and thus exclude immobilization as a possible type of

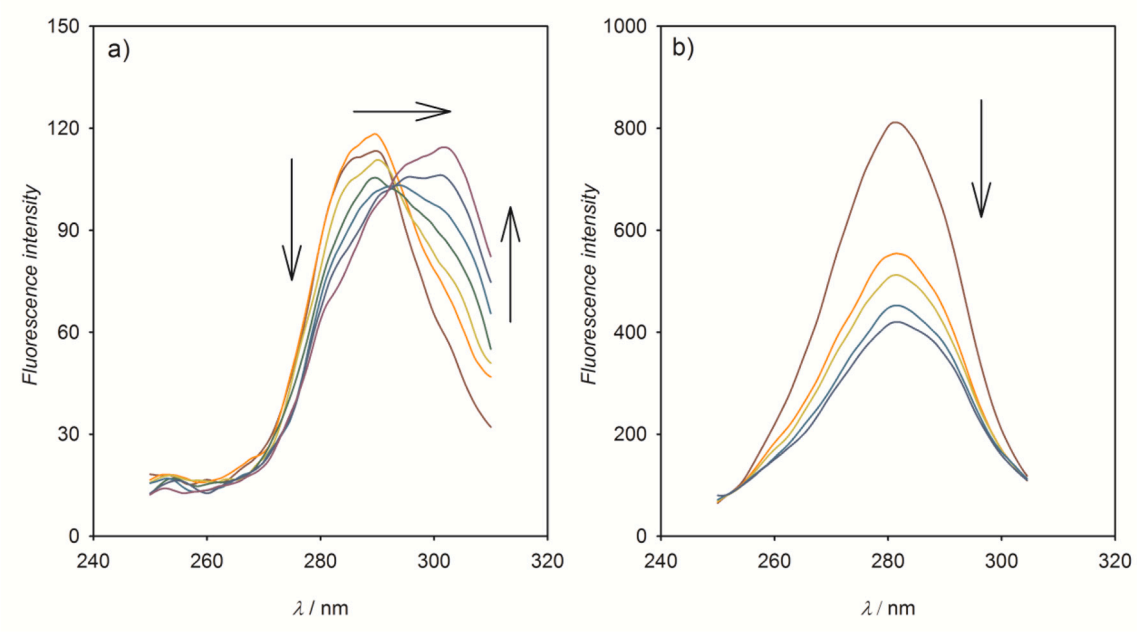

Fig. 9. Changes in synchronous emission spectra of BSA (1.1 μM) in 10 mM Tris-HCl buffer pH 7.42 in the absence and presence of an increasing concentration of (**1**): a) Δλ = 15 nm; b) Δλ = 60 nm.

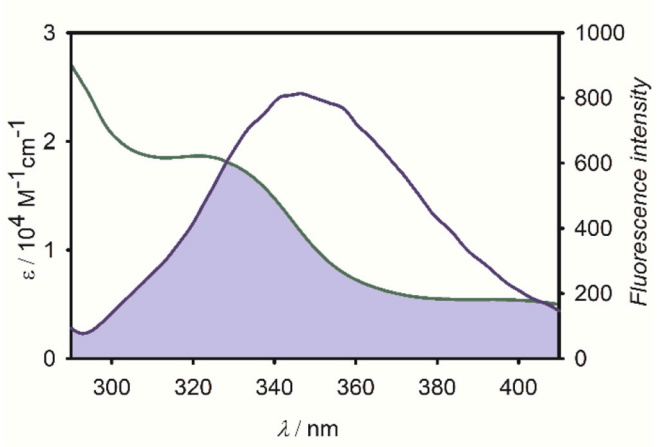

Fig. 10. Overlap of BSA emission spectrum and absorption spectrum of (**1**).

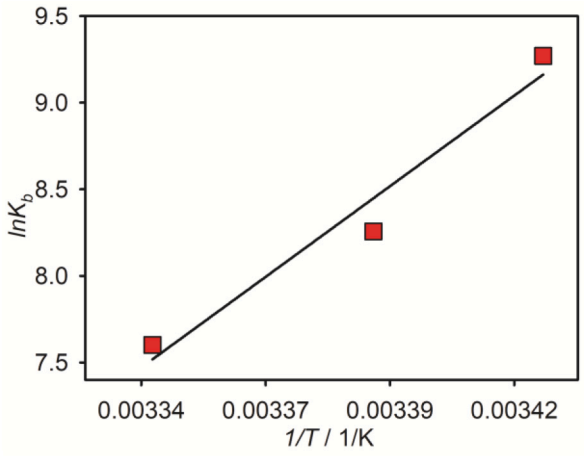

Fig. 11. The van't Hoff plot for interaction of complex (**4**) with BSA.

Table 6
FRET analysis data on BSA – vanadium complexes (**1**)–(**5**) interaction.

Complex	J / cm^3 M^{-1}	E	R_0 / nm	r / nm
(**1**)	1.569×10^{-14}	0.50	2.64	2.64
(**2**)	1.612×10^{-14}	0.66	2.65	2.37
(**3**)	1.755×10^{-14}	0.67	2.69	2.39
(**4**)	2.128×10^{-14}	0.70	2.78	2.41
(**5**)	1.805×10^{-14}	0.44	2.71	2.82

Table 7
Thermodynamic data on interaction of complex (**4**) with BSA.

T / K	K_{SV} / 10^5 M^{-1}	K_b / 10^3 M^{-1}	n	ΔH / kJ mol^{-1}	ΔS / J mol^{-1} K^{-1}	ΔG / kJ mol^{-1}
293.15	7.32	10.7	0.67			−22.3
295.15	3.77	3.85	0.64	−171	−510	−20.7
299.15	3.15	2.00	0.60			−18.7

the complex – BSA interaction. Negative values of enthalpy and entropy changes confirm that van der Waals interactions and hydrogen bonding dictate the nature of binding forces between (**4**) and BSA.

4. Conclusion

The reaction of stoichiometric amounts of [VO(acac)$_2$] with salicylaldehyde-based 2-furoic acid hydrazones and 2,2′-bipyridine in methanol yielded five novel heteroleptic neutral mononuclear oxidovanadium(IV) complexes of the general formula [VO(bpy)(hydrazonato-ONO)]. The paramagnetic d^1 V(IV) metal center, embedded in a tetragonally distorted bipyramid is hydrolytically inert and stabilized toward easy aerial oxidation. Swiss-ADME analysis showed the best drug-like properties for complex (**4**) featuring 5-nitro-salicildadehyde 2-furoic acid hydrazone ligand, which was selected for *in vivo* testing in healthy and diabetic Wistar rats. The increased levels of blood urea were observed for both, healthy and diabetic Wistar rats, compared to the control group indicating moderate renal toxicity. The

observed hypoalbuminemia in both groups of complex-treated rats is indicator of liver tissue impairment. However, the promising result is that complex (**4**) partially regulates streptozotocin-induced inflammatory activities in diabetic rats by inhibiting the activities of inflammatory cytokine and pro-inflammatory signaling since serum concentrations of globulins are lower in healthy rats treated with (**4**) compared to diabetic rats treated with (**4**). Finally, excellent antidiabetic effects of complex (**4**) were observed after only 7-days treatment of diabetic Wistar rats. Hypoalbuminemia *in vivo* inspired the investigation of complex – BSA interaction *in vitro*. The moderate affinity of the complexes for BSA with K_b values of 10^3–10^4 M^{-1} order distinguishes these complexes from generally albumin-reactive vanadium complexes, thus allowing reversible complex-albumin binding. Synchronous fluorescence spectra revealed the increased polarity in the microenvironment of tyrosine. FRET analysis suggested a static fluorescence quenching mechanism and non-radiative energy transfer. Thermodynamic data confirm van der Waals forces and hydrogen bonding as predominant types of interactions between complex and BSA. The results indicates that *in vitro* conditions the substituent on the hydrazone ligand has an influence on the binding of oxidovanadium(IV) complexes (**1**)–(**5**) with albumin. Further research of compound (**4**) will focus on the determination of the degree of liver and kidney injury for a chronic term *in vivo* application and examination of the effect of the substituent on the hydrazone ligand of oxidovanadium(IV) complexes on antidiabetic activity and hypoalbuminemia.

Funding

This work was supported by the Federal Ministry of Education and Science of Bosnia and Herzegovina under grant no. 05-35-1965-1/21 (Adnan Zahirović) and Croatian Science Foundation under the project HrZZ IP-2018-01-3168 (Dijana Žilić and Jurica Jurec).

Synopsis

Five novel neutral mononuclear heteroleptic vanadium(IV) complexes of salicylaldehyde-based furoic acid hydrazones are reported and fully characterised. Nitro derivative showed promising antidiabetic activity *in vivo* triggering mild hypoalbuminemia. Moderate affinity of complexes to albumin *in vitro* results with van der Waals interaction and hydrogen bonding as predominant binding modes.

CRediT authorship contribution statement

Adnan Zahirović: Conceptualization, Methodology, Investigation, Formal analysis, Visualization, Writing – original draft, Writing – review & editing, Supervision, Funding acquisition. **Selma Hadžalić:** Investigation, Formal analysis, Visualization. **Aleksandar Višnjevac:** Investigation, Writing – original draft. **Muhamed Fočak:** Investigation, Writing – original draft. **Burak Tüzün:** Methodology, Software, Writing – original draft. **Dijana Žilić:** Writing – original draft, Supervision, Funding acquisition. **Sunčica Roca:** Investigation, Writing – original draft, Writing – review & editing. **Jurica Jurec:** Investigation. **Anela Topčagić:** Investigation. **Irnesa Osmanković:** Investigation.

Declaration of Competing Interest

The authors declare that they have no known competing financial interests or personal relationships that could have appeared to influence the work reported in this paper.

Data availability

Data will be made available on request.

Acknowledgments

The numerical calculations reported in this paper were fully/partially performed at TUBITAK ULAKBIM, High Performance and Grid Computing Center (TRUBA resources). Authors are grateful to Dr. Amela Hozić and Dr. Mario Cindrić for their kindness in rapid providing the data on the mass spectra of complexes in aqueous solutions.

Appendix B. Supplementary data

Supplementary material associated with this article can be found in the online version. CCDC 2217484 contains the supplementary crystallographic data. These data can be obtained free of charge *via* http://www.ccdc.cam.ac.uk/conts/retrieving.html, or from the Cambridge Crystallographic Data Centre, 12 Union Road, Cambridge CB2 1EZ, UK; fax: (+44) 1223–336-033; or e-mail: deposit@ccdc.cam.ac.uk.

References

[1] K.H. Thompson, C. Orvig, Vanadium in diabetes: 100 years from Phase 0 to Phase I, J. Inorg. Biochem. 100 (2006) 1925–1935.
[2] J.J. Smee, J.A. Epps, G. Teissedre, M. Maes, N. Harding, L. Yang, B. Baruah, S. M. Miller, O.P. Anderson, G.R. Willsky, 4-amino-and 4-nitrodipicolinatovanadium (V) complexes and their hydroxylamido derivatives: synthesis, aqueous, and solid-state properties, Inorg. Chem. 46 (2007) 9827–9840.
[3] M. Li, J.J. Smee, W. Ding, D.C. Crans, Anti-diabetic effects of sodium 4-amino-2, 6-dipicolinatodioxovanadium (V) dihydrate in streptozotocin-induced diabetic rats, J. Inorg. Biochem. 103 (2009) 585–589.
[4] P. Buglyó, D.C. Crans, E.M. Nagy, R.L. Lindo, L. Yang, J.J. Smee, W. Jin, L.-H. Chi, M.E. Godzala, G.R. Willsky, Aqueous chemistry of the vanadiumIII (VIII) and the VIII– dipicolinate systems and a comparison of the effect of three oxidation states of vanadium compounds on diabetic hyperglycemia in rats, Inorg. Chem. 44 (2005) 5416–5427.
[5] A.B. Goldfine, M.E. Patti, L. Zuberi, B.J. Goldstein, R. LeBlanc, E.J. Landaker, C. R. Kahn, Metabolic effects of vanadyl sulfate in humans with non—insulin-dependent diabetes mellitus: in vivo and in vitro studies, Metab. 49 (2000) 400–410.
[6] K.H. Thompson, J. Lichter, C. LeBel, M.C. Scaife, J.H. McNeill, C. Orvig, Vanadium treatment of type 2 diabetes: a view to the future, J. Inorg. Biochem. 103 (2009) 554–558.
[7] S. Treviño, A. Díaz, E. Sánchez-Lara, B.L. Sanchez-Gaytan, J.M. Perez-Aguilar, E. González-Vergara, Vanadium in biological action: chemical, pharmacological aspects, and metabolic implications in diabetes mellitus, Biol. Trace Elem. Res. 188 (2019) 68–98.
[8] I. Goldwaser, S. Qian, E. Gershonov, M. Fridkin, Y. Shechter, Organic vanadium chelators potentiate vanadium-evoked glucose metabolism in vitro and in vivo: establishing criteria for optimal chelators, Mol. Pharmacol. 58 (2000) 738–746.
[9] K. Kawabe, Y. Yoshikawa, Y. Adachi, H. Sakurai, Possible mode of action for insulinomimetic activity of vanadyl (IV) compounds in adipocytes, Life Sci. 78 (2006) 2860–2866.
[10] Y. Yoshikawa, H. Sakurai, D.C. Crans, G. Micera, E. Garribba, Structural and redox requirements for the action of anti-diabetic vanadium compounds, Dalton Trans. 43 (2014) 6965–6972.
[11] T. Kiss, T. Jakusch, D. Hollender, Á. Dörnyei, É.A. Enyedy, J.C. Pessoa, A. Sanz-Medel, Biospeciation of antidiabetic VO (IV) complexes, Coord. Chem. Rev. 252 (2008) 1153–1162.
[12] M.M. Shakdofa, M.H. Shtaiwi, N. Morsy, T. Abdel-rassel, Metal complexes of hydrazones and their biological, analytical and catalytic applications: a review, Main Group Chem. 13 (2014) 187–218.
[13] A. Zahirović, I. Osmanković, A. Osmanović, A. Višnjevac, A. Magoda, S. Hadžalić, E. Kahrović, Interaction of copper (II) complexes of bidentate benzaldehyde nicotinic acid hydrazones with BSA: spectrofluorimetric and molecular docking approach, Acta Chim. Slov. 70 (2023) 74–85.
[14] É.A. Enyedy, L. Horváth, A. Hetényi, T. Tuccinardi, C.G. Hartinger, B.K. Keppler, T. Kiss, Interactions of the carrier ligands of antidiabetic metal complexes with human serum albumin: a combined spectroscopic and separation approach with molecular modeling studies, Bioorg. Med. Chem. 19 (2011) 4202–4210.
[15] A. Zahirović, S. Roca, E. Kahrović, A. Višnjevac, Low DNA and high BSA binding affinity of cationic ruthenium (II) organometallic featuring pyridine and 2′-hydroxychalcone ligands, J. Mol. Struct. 1236 (2021), 130326.
[16] K.G. Gurevich, Effect of blood protein concentrations on drug-dosing regimes: practical guidance, Theor. Biol. Med. Model. 10 (2013) 1–7.
[17] R.T. Scheife, Protein binding: what does it mean? Dicp 23 (1989) S27–S31.
[18] M. Liu, Z.J. Lim, Y.Y. Gwee, A. Levina, P.A. Lay, Characterization of a ruthenium (III)/NAMI-A adduct with bovine serum albumin that exhibits a high anti-metastatic activity, Angew. Chem. 122 (2010) 1705–1708.
[19] B.E. Bryant, W.C. Fernelius, D.H. Busch, R.C. Stoufer, W. Stratton, Vanadium (IV) oxy (acetylacetonate), Inorg. Synth. 5 (1957) 113–116.
[20] G.M. Sheldrick, Integrated space-group and crystal-structure determination, Acta Crystallogr. Sect. A: Found. Adv. 71 (2015) 3–8.
[21] G.M. Sheldrick, Crystal structure refinement with SHELXL, Acta Crystallogr. Sect. C: Struct. Chem. 71 (2015) 3–8.
[22] C.F. Macrae, I.J. Bruno, J.A. Chisholm, P.R. Edgington, P. McCabe, E. Pidcock, L. Rodriguez-Monge, R. Taylor, J. Streek, P.A. Wood, Mercury CSD 2.0–new

features for the visualization and investigation of crystal structures, J. Appl. Crystallogr. 41 (2008) 466–470.
[23] A.L. Spek, Structure validation in chemical crystallography, Acta Crystallogr. Sect. D: Biol. Crystallogr. 65 (2009) 148–155.
[24] L.J. Farrugia, WinGX and ORTEP for windows: an update, J. Appl. Crystallogr. 32 (1999) 837–838.
[25] A. Syamal, M. Maurya, Salicylaldehyde-2-furoic acid hydrazide as a chelating ligand: complexes with nickel (II), cobalt (II), copper (II), zinc (II), zirconium (IV), oxomolybdenum (V) & dioxouranium (VI), Indian J. Chem. 24A (1985) 836–840.
[26] E.G. Hohenstein, S.T. Chill, C.D. Sherrill, Assessment of the performance of the M05− 2X and M06− 2X exchange-correlation functionals for noncovalent interactions in biomolecules, J. Chem. Theory Comput. 4 (2008) 1996–2000.
[27] A.D. Becke, Density-functional thermochemistry. I. The effect of the exchange-only gradient correction, J. Chem. Phys. 96 (1992) 2155–2160.
[28] M. Frisch, G. Trucks, H. Schlegel, G. Scuseria, M. Robb, J. Cheeseman, G. Scalmani, V. Barone, B. Mennucci, G. Petersson, Gaussian 09, Revision A.02. Inc, Wallingford, CT, 2009.
[29] R. Dennington, T.A. Keith, J.M. Millam, GaussView 6.0. 16 Semichem Inc, Shawnee Mission, KS, USA, 2016.
[30] M. Rezaeivala, M. Bozorg, N. Rafiee, K. Sayin, B. Tuzun, Corrosion inhibition of carbon steel using a new morpholine-based ligand during acid pickling: experimental and theoretical studies, Inorg. Chem. Commun. 148 (2023), 110323.
[31] S. Daoui, Ş. Direkel, M.M. Ibrahim, B. Tüzün, T. Chelfi, M. Al-Ghorbani, M. Bouatia, M.E. Karbane, A. Doukkali, N. Benchat, Synthesis, spectroscopic characterization, antibacterial activity, and computational studies of novel pyridazinone derivatives, Molecules. 28 (2023) 678.
[32] M. Chalkha, A.A. el Hassani, A. Nakkabi, B. Tüzün, M. Bakhouch, A.T. Benjelloun, M. Sfaira, M. Saadi, L. El Ammari, M. El Yazidi, Crystal structure, Hirshfeld surface and DFT computations, along with molecular docking investigations of a new pyrazole as a tyrosine kinase inhibitor, J. Mol. Struct. 1273 (2023), 134255.
[33] A. Daina, O. Michielin, V. Zoete, SwissADME: a free web tool to evaluate pharmacokinetics, drug-likeness and medicinal chemistry friendliness of small molecules, Sci. Rep. 7 (2017) 42717.
[34] A. Kenđel, S. Miljanić, D. Kontrec, Ž. Soldin, N. Galić, Copper (II) complexes of aroylhydrazones: preparation and structural characterization, J. Mol. Struct. 1207 (2020), 127783.
[35] S.Y. Ebrahimipour, I. Sheikhshoaie, A.C. Kautz, M. Ameri, H. Pasban-Aliabadi, H. A. Rudbari, G. Bruno, C. Janiak, Mono-and dioxido-vanadium (V) complexes of a tridentate ONO Schiff base ligand: synthesis, spectral characterization, X-ray crystal structure, and anticancer activitY, Polyhedron. 93 (2015) 99–105.
[36] M. Kuriakose, M.P. Kurup, E. Suresh, Synthesis, spectroscopic studies and crystal structures of two new vanadium complexes of 2-benzoylpyridine containing hydrazone ligands, Polyhedron. 26 (2007) 2713–2718.
[37] P.A. Lakshmi, T. Satyanarayana, P.S. Reddy, Synthesis, characterization and antimicrobial activity of oxovanadium (IV) complexes of Schiff base hydrazones containing quinoxaline moiety, Chin. J. Chem. 30 (2012) 935–940.
[38] P. Sreeja, M.P. Kurup, Synthesis and spectral characterization of ternary complexes of oxovanadium (IV) containing some acid hydrazones and 2, 2′-bipyridine, Spectrochim. Acta, Part A. 61 (2005) 331–336.
[39] P. Paciorek, J. Szklarzewicz, A. Jasińska, B. Trzewik, W. Nitek, M. Hodorowicz, Synthesis, structural characterization and spectroscopy studies of new oxovanadium (IV, V) complexes with hydrazone ligands, Polyhedron. 87 (2015) 226–232.
[40] E. Seena, N. Mathew, M. Kuriakose, M.P. Kurup, Synthesis, spectral and EPR studies of oxovanadium (IV) complexes incorporating tridentate ONO donor hydrazone ligands: structural study of one oxovanadium (V) complex, Polyhedron. 27 (2008) 1455–1462.
[41] Y. Dong, R.K. Narla, E. Sudbeck, F.M. Uckun, Synthesis, X-ray structure, and anti-leukemic activity of oxovanadium (IV) complexes, J. Inorg. Biochem. 78 (2000) 321–330.
[42] S. Stoll, A. Schweiger, EasySpin, a comprehensive software package for spectral simulation and analysis in EPR, J. Magn. Reson. 178 (2006) 42–55.
[43] I.V. Kurganskii, E.S. Bazhina, A.A. Korlyukov, K.A. Babeshkin, N.N. Efimov, M. A. Kiskin, S.L. Veber, A.A. Sidorov, I.L. Eremenko, M.V. Fedin, Mapping magnetic properties and relaxation in vanadium (IV) complexes with lanthanides by electron paramagnetic resonance, Molecules. 24 (2019) 4582.
[44] B. Szymańska, D. Skrzypek, D. Kovala-Demertzi, M. Staninska, M.A. Demertzis, Synthesis and spectroscopic study of copper (II) and manganese (II) complexes with pipemidic acid, Spectrochim. Acta, Part A 63 (2006) 518–523.
[45] J. Krzystek, A. Ozarowski, J. Telser, D.C. Crans, High-frequency and-field electron paramagnetic resonance of vanadium (IV, III, and II) complexes, Coord. Chem. Rev. 301 (2015) 123–133.
[46] I.E. Soshnikov, N.V. Semikolenova, A.A. Shubin, K.P. Bryliakov, V.A. Zakharov, C. Redshaw, E.P. Talsi, EPR monitoring of vanadium (IV) species formed upon activation of vanadium (V) polyphenolate precatalysts with AlR2Cl and AlR2Cl/ethyltrichloroacetate (R= Me, Et), Organometallics. 28 (2009) 6714–6720.
[47] J. Szklarzewicz, A. Jurowska, M. Hodorowicz, R. Gryboś, K. Kruczała, M. Głuch-Lutwin, G. Kazek, Vanadium complexes with salicylaldehyde-based Schiff base ligands—structure, properties and biological activity, J. Coord. Chem. 73 (2020) 986–1008.
[48] J. Szklarzewicz, A. Jurowska, M. Hodorowicz, G. Kazek, M. Głuch-Lutwin, J. Sapa, M. Papież, Tridentate ONO ligands in vanadium (III-V) complexes-synthesis, characterization and biological activity, J. Mol. Struct. 1224 (2021), 129205.
[49] J. Szklarzewicz, A. Jurowska, M. Hodorowicz, G. Kazek, M. Głuch-Lutwin, J. Sapa, Ligand role on insulin-mimetic properties of vanadium complexes. Structural and biological studies, Inorg. Chim. Acta 516 (2021), 120135.
[50] R. Gryboś, J. Szklarzewicz, A. Jurowska, M. Hodorowicz, Properties, structure and stability of V (IV) hydrazide Schiff base ligand complex, J. Mol. Struct. 1171 (2018) 880–887.
[51] H. Hosseini Monfared, R. Bikas, P. Anarjan, A. Blake, N. Burcu Arslan, C. Kazak, V. Lippolis, Oxidovanadium (V) complexes containing hydrazone based O, N, O-donor ligands: synthesis, structure, catalytic properties and theoretical calculations, Polyhedron. 69 (2014) 90–102.
[52] J. Szklarzewicz, A. Jurowska, D. Matoga, K. Kruczała, G. Kazek, B. Mordyl, J. Sapa, M. Papież, Synthesis, coordination properties and biological activity of vanadium complexes with hydrazone Schiff base ligands, Polyhedron. 185 (2020), 114589.
[53] C.L. Simpson, C.G. Pierpont, Complexes of vanadium (III) and vanadium (IV) containing bipyridine and tetrachlorocatecholate ligands. Insights into the tunicate vanadium (III) coordination environment, Inorg. Chem. 31 (1992) 4308–4313.
[54] I. Shahzadi, A.F. Zahoor, B. Tüzün, A. Mansha, M.N. Anjum, A. Rasul, A. Irfan, K. Kotwica-Mojzych, M. Mojzych, Repositioning of acefylline as anti-cancer drug: synthesis, anticancer and computational studies of azomethines derived from acefylline tethered 4-amino-3-mercapto-1, 2, 4-triazole, PLoS One 17 (2022), e0278027.
[55] E. Önem, B. Tüzün, S. Akkoç, Anti-quorum sensing activity in Pseudomonas aeruginos a PA01 of benzimidazolium salts: electronic, spectral and structural investigations as theoretical approach, J. Biomol. Struct. Dyn. 40 (2022) 6845–6856.
[56] C.A. Lipinski, F. Lombardo, B.W. Dominy, P.J. Feeney, Experimental and computational approaches to estimate solubility and permeability in drug discovery and development settings, Adv. Drug Deliv. Rev. 23 (1997) 3–25.
[57] L. Guan, H. Yang, Y. Cai, L. Sun, P. Di, W. Li, G. Liu, Y. Tang, ADMET-score–a comprehensive scoring function for evaluation of chemical drug-likeness, MedChemComm 10 (2019) 148–157.
[58] A.K. Ghose, V.N. Viswanadhan, J.J. Wendoloski, A knowledge-based approach in designing combinatorial or medicinal chemistry libraries for drug discovery. 1. A qualitative and quantitative characterization of known drug databases, J. Comb. Chem. 1 (1999) 55–68.
[59] H. Pajouhesh, G.R. Lenz, Medicinal chemical properties of successful central nervous system drugs, NeuroRx 2 (2005) 541–553.
[60] B. Bakchi, A.D. Krishna, E. Sreecharan, V.B.J. Ganesh, M. Niharika, S. Maharshi, S. B. Puttagunta, D.K. Sigalapalli, R.R. Bhandare, A.B. Shaik, An overview on applications of SwissADME web tool in the design and development of anticancer, antitubercular and antimicrobial agents: a medicinal chemist's perspective, J. Mol. Struct. 132712 (2022).
[61] O. Alaysuy, H.M. Abumelha, A. Alsoliemy, A. Alharbi, N.M. Alatawi, H.E. Osman, R. Zaky, N.M. El-Metwaly, Elucidating of new hydrazide-based complexes derived from Pd (II), Cu (II) and Cd (II) ions: studies concerning spectral, DFT, Hirshfeld-crystal, biological screening beside Swiss-ADME verification, J. Mol. Struct. 1259 (2022), 132748.
[62] A.K. Srivastava, Anti-diabetic and toxic effects of vanadium compounds, Mol. Cell. Biochem. 206 (2000) 177–182.
[63] M. Younes, O. Strubelt, Vanadate-induced toxicity towards isolated perfused rat livers: the role of lipid peroxidation, Toxicol. 66 (1991) 63–74.
[64] L. Yang, M. Liao, Influence of myrcene on inflammation, matrix accumulation in the kidney tissues of streptozotocin-induced diabetic rat, Saudi, J. Biol. Sci. 28 (2021) 5555–5560.
[65] S.P. Dash, A.K. Panda, S. Dhaka, S. Pasayat, A. Biswas, M.R. Maurya, P.K. Majhi, A. Crochet, R. Dinda, A study of DNA/BSA interaction and catalytic potential of oxidovanadium (V) complexes with ONO donor ligands, Dalton Trans. 45 (2016) 18292–18307.
[66] S.A. Patra, A. Banerjee, G. Sahu, M. Mohanty, S. Lima, D. Mohapatra, H. Görls, W. Plass, R. Dinda, Evaluation of DNA/BSA interaction and in vitro cell cytotoxicity of μ2-oxido bridged divanadium (V) complexes containing ONO donor ligands, J. Inorg. Biochem. 233 (2022), 111852.
[67] A. Banerjee, S.P. Dash, M. Mohanty, D. Sanna, G. Sciortino, V. Ugone, E. Garribba, H. Reuter, W. Kaminsky, R. Dinda, Chemistry of mixed-ligand oxidovanadium (IV) complexes of aroylhydrazones incorporating quinoline derivatives: study of solution behavior, theoretical evaluation and protein/DNA interaction, J. Inorg. Biochem. 199 (2019), 110786.
[68] G. Sahu, S.A. Patra, M. Mohanty, S. Lima, P.D. Pattanayak, W. Kaminsky, R. Dinda, Dithiocarbazate based oxidomethoxidovanadium (V) and mixed-ligand oxidovanadium (IV) complexes: study of solution behavior, DNA binding, and anticancer activity, J. Inorg. Biochem. 233 (2022), 111844.
[69] S. Lima, A. Banerjee, G. Sahu, S.A. Patra, K. Sahu, T. Sasamori, G. Sciortino, E. Garribba, R. Dinda, New mixed ligand oxidovanadium (IV) complexes: solution behavior, protein interaction and cytotoxicity, J. Inorg. Biochem. 233 (2022), 111853.
[70] A. Zahirović, D. Žilić, S.K. Pavelić, M. Hukić, S. Muratović, A. Harej, E. Kahrović, Type of complex–BSA binding forces affected by different coordination modes of alliin in novel water-soluble ruthenium complexes, New J. Chem. 43 (2019) 5791–5804.
[71] S.D. Kurbah, A. Kumar, I. Syiemlieh, R.A. Lal, Pi-pi interaction and hydrogen bonding in crystal structure of vanadium (V) complex containing mono hydrazone ligand: synthesis and protein binding studies, Inorg. Chem. Commun. 86 (2017) 6–9.
[72] M. Kongot, N. Dohare, D.S. Reddy, N. Pereira, R. Patel, M. Subramanian, A. Kumar, In vitro apoptosis-induction, antiproliferative and BSA binding studies of a oxidovanadium (V) complex, J. Trace Elem. Med. Biol. 51 (2019) 176–190.
[73] A. Kumar, S.D. Kurbah, I. Syiemlieh, S.A. Dhanpat, R. Borthakur, R.A. Lal, Synthesis, characterization, reactivity, and catalytic studies of heterobimetallic

vanadium (V) complexes containing hydrazone ligands, Inorg. Chim. Acta 515 (2021), 120068.
[74] S.P. Dash, A.K. Panda, S. Pasayat, S. Majumder, A. Biswas, W. Kaminsky, S. Mukhopadhyay, S.K. Bhutia, R. Dinda, Evaluation of the cell cytotoxicity and DNA/BSA binding and cleavage activity of some dioxidovanadium (V) complexes containing aroylhydrazones, J. Inorg. Biochem. 144 (2015) 1–12.
[75] B.K. Biswas, N. Biswas, S. Saha, A. Rahaman, D.P. Mandal, S. Bhattacharjee, N. Sepay, E. Zangrando, E. Garribba, C.R. Choudhury, Interaction with bioligands and in vitro cytotoxicity of a new dinuclear dioxido vanadium (V) complex, J. Inorg. Biochem. 237 (2022), 111980.
[76] M. Memišević, A. Zahirović, A. Višnjevac, A. Osmanović, D. Žilić, M. Kralj, S. Muratović, I. Martin-Kleiner, D. Završnik, E. Kahrović, Copper (II) salicylideneimine complexes revisited: from a novel derivative and extended characterization of two homologues to interaction with BSA and antiproliferative activity, Inorg. Chim. Acta 525 (2021), 120460.
[77] D. İnci, R. Aydın, Ö. Vatan, T. Sevgi, D. Yılmaz, Y. Zorlu, Y. Yerli, B. Çoşut, E. Demirkan, N. Çinkılıç, Synthesis and crystal structures of novel copper (II) complexes with glycine and substituted phenanthrolines: reactivity towards DNA/BSA and in vitro cytotoxic and antimicrobial evaluation, JBIC, J. Biol. Inorg. Chem. 22 (2017) 61–85.
[78] Y.Z. Zhang, X.X. Chen, J. Dai, X.P. Zhang, Y.X. Liu, Y. Liu, Spectroscopic studies on the interaction of lanthanum (III) 2-oxo-propionic acid salicyloyl hydrazone complex with bovine serum albumin, Lumin. 23 (2008) 150–156.
[79] C. Barakat, D. Patra, Combining time-resolved fluorescence with synchronous fluorescence spectroscopy to study bovine serum albumin-curcumin complex during unfolding and refolding processes, Lumin. 28 (2013) 149–155.
[80] S. Li, K. Huang, M. Zhong, J. Guo, W.-Z. Wang, R. Zhu, Comparative studies on the interaction of caffeic acid, chlorogenic acid and ferulic acid with bovine serum albumin, Spectrochim. Acta, Part A 77 (2010) 680–686.
[81] S.A. Patra, M. Mohanty, A. Banerjee, S. Kesarwani, F. Henkel, H. Reuter, R. Dinda, J., Protein binding and cytotoxic activities of monomeric and dimeric oxido-vanadium (V) salan complexes: exploring the solution behavior of monoalkoxido-bound oxido-vanadium (V) complex, Inorg. Biochem. 224 (2021), 111582.
[82] G. Sahu, A. Banerjee, R. Samanta, M. Mohanty, S. Lima, E.R. Tiekink, R. Dinda, Water-soluble dioxidovanadium (V) complexes of aroylhydrazones: DNA/BSA interactions, hydrophobicity, and cell-selective anticancer potential, Inorg. Chem. 60 (2021) 15291–15309.
[83] P.D. Ross, S. Subramanian, Thermodynamics of protein association reactions: forces contributing to stability, Biochem. 20 (1981) 3096–3102.
[84] J.M. Mollerup, A review of the thermodynamics of protein association to ligands, protein adsorption, and adsorption isotherms, Chem. Eng. Technol. 31 (2008) 864–874.